# REMOTE SENSING OF WATER QUALITY IN ROTORUA AND WAIKATO LAKES

A thesis submitted in partial fulfillment

of the requirements for the degree

of

**Master of Science in Biological Sciences**

at

**The University of Waikato**

by

**MATHEW GRANT ALLAN**


THE UNIVERSITY OF
WAIKATO
*Te Whare Wānanga o Waikato*

**2008**

# Abstract

Remote sensing has the potential to monitor spatial variation in water quality over large areas. While ocean colour work has developed analytical bio-optical water quality retrieval algorithms for medium spatial resolution platforms, remote sensing of lake water is often limited to high spatial resolution satellites such as Landsat, which have limited spectral resolution. This thesis presents the results of an investigation into satellite monitoring of lake water quality. The aim of this investigation was to ascertain the feasibility of estimating water quality and its spatial distribution using Landsat 7 ETM+ imagery combined with *in situ* data from Rotorua and Waikato lakes. For the comparatively deep Rotorua lakes, $r^2$ values of 0.91 (January 2002) and 0.83 (March 2002) were found between *in situ* chlorophyll (chl) *a* and the Band1/Band3 ratio. This technique proved useful for analysing the spatial distribution of phytoplankton, especially in lakes Rotoiti and Rotoehu. For the more bio-optically complex shallow lakes of the Waikato, a linear spectral unmixing (LSU) approach was investigated where the water surface reflectance spectrum is defined by the contribution from pure pixels or endmembers. The model estimates the percentage of the endmember within the pixel, which is then used in a final regression with *in situ* data to map water quality in all pixels. This approach was used to estimate the concentration of chl *a* ($r^2 = 0.84$). Total suspended solid (TSS) concentration was mapped using the traditional Band 3 regression with *in situ* data, which combined atmospherically corrected reflectance for both images into a single relationship ($r^2 = 0.98$). The time difference between *in situ* data collection and satellite data capture is a potential source of error. Other potential sources of error

include sample location accuracy, the influence of dissolved organic matter, and masking of chl *a* signatures by high concentrations of TSS. The results from this investigation suggest that remote sensing of water quality provides meaningful and useful information with a range of applications and could provide information on temporal spatial variability in water quality.

# Acknowledgements

First and foremost thanks to my supervisors Brendan Hicks and Lars Brabyn for all their time and effort.

This work was funded by the Foundation for Research, Science and Technology contract UOWX0505. I thank Environment Bay of Plenty for providing the measured data of water quality variables. Glenn Ellery, Paul Scholes, and Gareth Evans from Environment Bay of Plenty, also assisted. David Hamilton (University of Waikato) provided constructive advice on model development and the manuscript content. David Burger and Chris McBride helped with data collection. Salman Ashraf provided technical support. Kevin Collier (Environment Waikato) also provided valuable advice and comments. For Chapter 3, Environment Waikato supplied *in situ* data, and for this I thank especially Derrick Phyn and Ian Buchanan. Thanks to Grant Tempero for all your advice and help editing this thesis.

# Table of Contents

# List of Tables

# List of Figures

# List of Appendices

# 1. Introduction

## 1.1 Remote sensing

Remote sensing is the science of obtaining information about an object using a device that is not in contact with that object. According to this definition, remote sensing has been practiced by the pioneers of astronomy such as Galileo and Copernicus. Modern environmental remote sensing has its roots in the military reconnaissance of World War I. From this point on, remote sensing benefited from technological advances emerging from space exploration programs (Bukata *et al*., 1995). The present study uses images acquired by satellites to investigate water quality by ground-truthing electromagnetic information with physical measurements.

The radiance (L) recorded by a remote sensor includes four components (Figure. 1.1), comprising:

L*a*: downwelling solar and sky radiation that does not contact the air-water interface, which represents contribution from the atmosphere. The gases $O_2$, $CO_2$, and $H_2O$ and aerosols (liquid or solid) present in the atmosphere scatter and absorb radiation.

L*s*: reflection from the aquatic surface (air-water interface), often seen as sun glints where the data is deteriorated to such an extent that is unusable.

L*v*: downwelling sky and solar radiation that penetrates the air water-interface and re-emerges from the water without contacting the bottom of the water body.

L*b*: downwelling sky and solar radiation that penetrates the air water-interface, reaches the bottom, and re-emerges from the water column (Bukata *et al*., 1995).

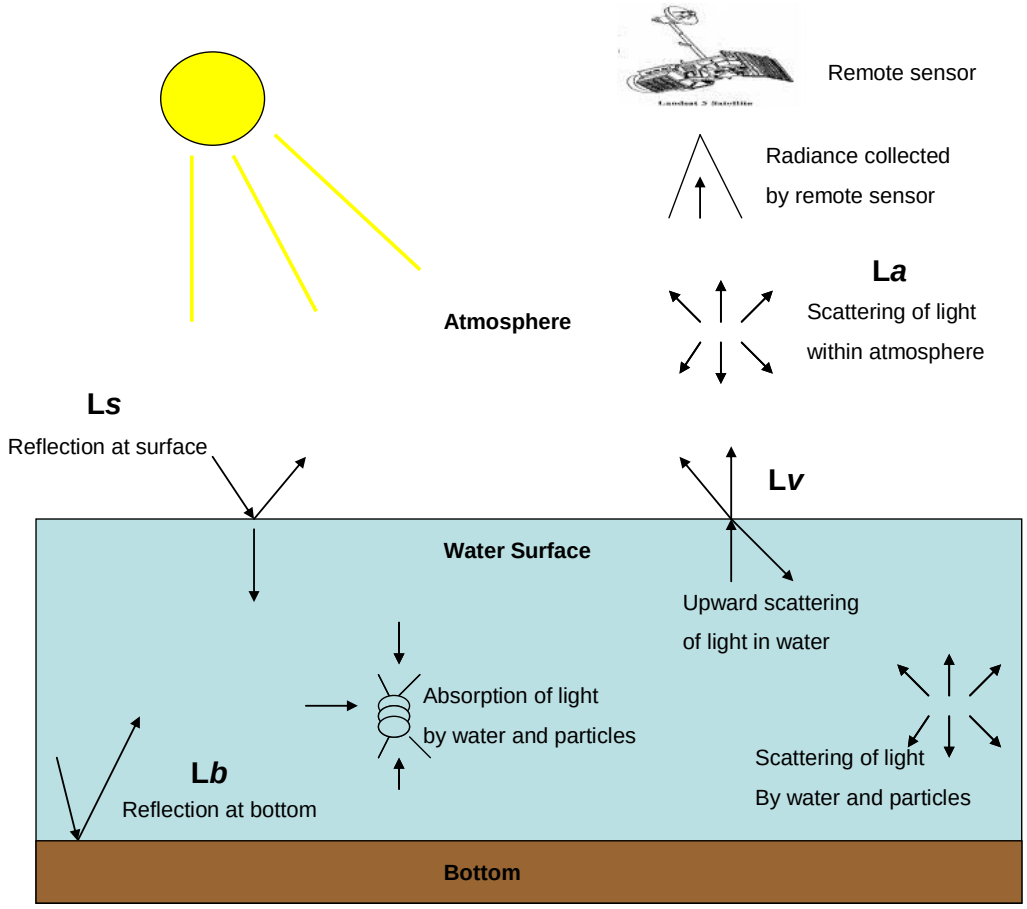


Figure 1.1. The different origins of light received by a remote sensor. Source: Adapted from Kirk (1994).

## 1.2 Water colour and quality

This study focuses on optical water quality which can be defined as follows (Kirk 1988):

> *'The extent to which the suitability of water for its functional role in the biosphere or the human environment is determined by its optical properties.'*

The main aspects that affect the visual appearance of waters are clarity and colour. Clarity includes visual clarity and the extent of light penetration into water. Colour can be described in terms of hue (blue, green, yellow, etc.), colour purity (ranging

from neutral grays to spectral colours), and brightness related to back scattering (Davies-Colley *et al*., 1993).

The colour and clarity of water depends on its optical character, relating to the bulk optical processes occurring in water of absorption and scattering. Absorption refers to the transfer of light energy into another form and is quantified by the absorption coefficient, *a*, which is the fraction of incident light which is absorbed divided by the thickness of the layer. Scattering is defined as the change in direction of light photons (Davies-Colley *et al*., 1993), and is quantified by the scattering coefficient, *b*, which is the fraction of the incident light which is scattered divided by the thickness of the layer (Kirk, 1994). Total attenuation is given by the beam attenuation coefficient:

$$c = a + b \qquad \text{equation 1.1,}$$

These are referred to as inherent optical properties (IOPs) as they are dependant on optically active substances comprising the aquatic medium. In contrast apparent optical properties (AOPs) are affected by the geometric structure of the light field and water constituents (Kirk, 1994). AOPs include the reflectance recorded by remote sensing devices, as it is dependant on the radiance distribution of the light regime. These properties are partly determined by the solar zenith angle and local atmospheric conditions (Bukata *et al*., 1995). Secchi depth is the most familiar AOP (Preisendorfer, 1961).

Fluorescence is another optical process which involves the absorption of part of the energy of a light photon and re-radiation of a lower energy photon in an arbitrary direction, which can sometimes influence the colour of natural waters (Davies-Colley *et al*., 1993).

Optically active substances (OAS) found in water affect the reflected energy emitted by water bodies, therefore analysis of this data leads to estimates of concentrations of these substances. The main OAS in lake water are chlorophyll (chl) *a*, suspended minerals, and dissolved organic matter (DOM) (Bukata *et al*., 1995).

Clear water contains low concentrations of these optically active substances, and consequently the spectral reflectance is low and the spectral shape is similar to

that of pure water molecules, where there is an exponential increase in absorption towards longer wavelengths, and an increase in scattering at shorter wavelengths of the visible near infrared (Figure 1.2) (Rurdorff *et al*., 2007).

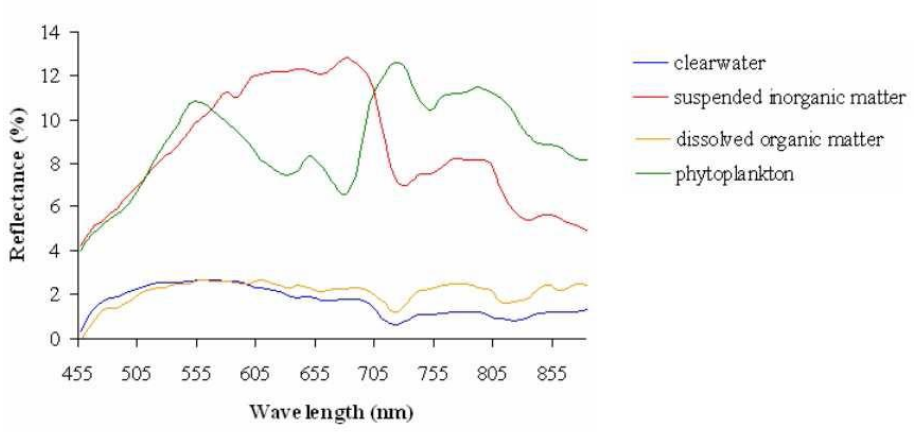


Figure 1.2. Spectrographic signatures of different water types. Source: Rurdorff *et al*., (2007).

Algae-laden water exhibits a reflectance peak in the green region (Figure 1.2), which represents an aggregate absorption minimum, and another reflectance peak at 700 nm. Also absorption troughs can be seen in the blue and red/infrared wavelengths (Han, 1997), although the exact location and width of these troughs depend on the phytoplankton species and their physiological state (Kirk, 1983). Phytoplankton displays fluorescence with a peak centered at 685 nm, meaning concentration can be measured using fluorometers (Yentsch and Yentsch, 1979).

Suspended sediment (SS) includes sand, silt, clay and other inorganic material such as atmospheric dust (Koponen, 2006). The optical properties of inorganic sediment are affected by their shape and size distribution, and have a major effect on their absorption and scattering properties (Bukata *et al*., 1995). Due to the complexity of determining concentrations of inorganic sediment it is more common

that total suspended solids (TSS) are measured, which includes both organic and inorganic sediment. In clear water, increasing concentrations of SS results in a linear increase in reflectance in the infrared, with a coefficient of variation near to one. In this area of the electromagnetic spectrum the effect of chl *a* is negligible (Han, 1997). In algae-laden water, the additive effects of SS on reflectance occur at all wavelengths.

The absorption spectrum of DOM has an exponential function at visible wavelengths with increasing absorption at shorter wavelengths and little absorption above 700 nm (Bricaud *et al*., 1981). As the substances are dissolved the effect of scattering can be ignored (Koponen, 2006).

## 1.3 Problem statement

Traditional water sampling methods are able to quantify temporal changes in water quality at specific points. However, they are unable to effectively quantify water quality across the entire surface area. In lakes with high spatial variation point samples are often not representative of the whole water body, which can produce errors. Also, due the expense of traditional water quality monitoring, often, only selected water bodies are monitored. The advantage of remote sensing is that large areas of ground can be covered simultaneously, and water quality can be estimated over a much greater area.

## 1.4 Conceptual solution

In the Rotorua lakes where chl *a* is often the dominant colour producing agent, it is proposed that using traditional remote sensing methods to relate remote sensing signals to *in situ* data using regression analysis should be effective in determining chl *a* and Secchi depth. In the more optically complex Waikato lakes where a mixture of high concentrations of TSS, chl *a*, and DOM are present, a linear spectral unmixing model will be used for the retrieval of chl *a* concentrations.

## 1.5 Aim and objectives

The aim of this study was to examine the feasibility of determining water quality from Landsat 7 ETM+ imagery. Its objectives were:

1) To compare chl *a* and Secchi depth measurements in the Rotorua lakes to band intensity using traditional band ratio methods and regression methods.

2) To determine suspended solids in the Waikato lakes using Landsat Band 3.

3) To determine chl *a* in the Waikato lakes using linear spectral unmixing.

## 1.6 Structure of thesis

The first chapter introduces remote sensing and the underlying principles of remote sensing for water quality. The research question is defined and the aim and objectives were explained. The second and third chapter form independent studies. Chapter 2 presents an investigation of remote sensing for water quality in the Rotorua lakes using traditional band ratio methods. Chapter 3 presents an investigation of remote sensing for water quality in the Waikato lakes, using linear spectral unmixing. Chapter 4 includes a general conclusion.

# 2. Rotorua lakes

## 2.1 Introduction

The aim of remote sensing of lakes is to provide truly synoptic monitoring of water quality. Traditional point sampling using chemical and meter methods can be expensive and effectively monitor the heterogeneity of water quality variables (Dekker *et al*., 2002). Operational remote sensing of the ocean originated from the launch of the Coastal Zone Color Scanner in 1978 and the subsequent development of empirical blue green band ratio models for the remote estimation of Chlorophyll (chl) *a*. The data from this satellite provided the first maps of the global distribution of chl *a* (Abbott and Chelton, 1991). This was followed by the launch of other successful ocean colour satellites such as MODIS and SeaWiFS. Inland remote sensing of small lakes requires a higher resolution platform, and of these platforms the most commonly used to study water quality is the Landsat series of satellites.

Table 2.1. Landsat 7 ETM+ band specifications (NASA specification table).

| Band number | Spectral range (μm) | Ground resolution (m) |
|---|---|---|
| B1 | 0.450 to 0.515 | 30 |
| B2 | 0.525 to 0.605 | 30 |
| B3 | 0.630 to 0.690 | 30 |
| B4 | 0.750 to 0.900 | 30 |
| B5 | 1.55 to 1.75 | 30 |
| B6 | 10.4 to 12.5 | 60 |
| B7 | 2.09 to 2.35 | 30 |
| Panchromatic | 0.520 to 0.900 | 15 |

Landsat Multispectral Scanner (MSS) imagery is available from 1972-1981, Landsat 5 Thematic Mapper (TM) was launched in 1984 and is still operating, and Landsat 7 Enhanced Thematic Mapper + (ETM+) was launched in 1999 ( Table 2.1). The repeat cycle is 16 days, and each scene is 185 km wide and 120 km high (Table 2.2).

Landsat satellites record digital images of lakes and their catchments by recording electromagnetic radiation at distinct wavelengths or bands (Table 2.1). The highest correlation between water quality variables and satellite signatures is found in the visible (0.4-0.7 μm) and near infra red (0.7-1.5 μm) spectrum which corresponds to Landsat bands 1- 4 (Curran 1985). The main factors that affect water clarity are chl *a*, suspended sediments (SS), and dissolved organic matter (DOM). These factors subsequently affect the water subsurface radiance reflectance measured by satellites (Bukata *et al.*, 1995).

Table 2.2. Landsat 7 ETM+ capabilities (NASA specification table).

| Attribute | Value |
|---|---|
| Swath width: | 185 km |
| Repeat coverage interval: | 16 days (233 orbits) |
| Altitude: | 705 km |
| Quantization: | Best 8 of 9 bits |
| On-board data storage: | ~375 Gb (solid state) |
| Inclination: | Sun-synchronous, 98.2 degrees |
| Equatorial crossing: | Descending node; 10:00am +/- 15 min. |
| Launch vehicle: | Delta II |
| Launch date: | April 1999 |

Chl *a* acts primarily as a differential absorber, causing a decrease in the spectral response at the blue end (450-520 nm) of the visible spectrum. SS are associated

with increases in reflected energy at longer red wavelengths (630-690 nm) (Bukata *et al.,* 1995).

The dominant factors that affect water clarity in the Rotorua lakes have been found to be algal biomass and SS. Algal biomass was the dominant influence on water clarity in Lake Okaro (accounting for 68% of the variability), whereas Lake Rotorua water clarity was more often dominated by SS, although chl *a* was occasionally predominant (Vant and Davies-Colley, 1986).

Reliable estimates of lake water quality from remote sensing can be achieved without employing *in situ* data, but accuracy of estimates can be improved by using reference data for a limited number of lakes (Pulliainen *et al.,* 2001). Accurate estimates of spatial variation in water quality in the Rotorua lakes may be possible using only a few *in situ* samples to calibrate models.

The Rotorua lakes are of recent volcanic origin (140,000 years old) and were mostly formed by explosion craters or as the result of subsidence associated with volcanic activity (Lowe and Green, 1986). There are 12 main lakes in the Rotorua area that represent a wide range of lake geomorphology and water quality. This makes it suitable for remote sensing, as regression models cover a wide range of water quality (Olmanson *et al.,* 2001).

The Rotorua lakes fit into four categories based on their mixing regimes and trophic status. These are eutrophic monomictic (Okaro and Rotoiti), mesotrophic monomictic (Okareka, Tikitapu, Rotokakahi and Okataina), oligotrophic monomictic (Tarawera, Rotoma, and Rotomahana) and meso- and eutrophic polymictic lakes (Rotorua, Rotoehu, and Rerewhakaaitu) (Hamilton 2003).

Numerous investigations have shown that strong empirical relationships can be developed between Landsat Multispectral Scanner (MSS) or Thematic Mapper (TM) imagery and *in situ* measurements of water quality (Table 2.3). One of the first studies of lakes with satellites used MSS images in a reconnaissance analysis of lake condition in Minnesota (Brown *et al.*, 1977). Later, Landsat imagery was used to generate a reliable prediction for chl *a* concentration in the Minnesota lakes, USA (Lillesand *et al.*, 1983). Also determinations of long term Secchi depth trends from 13 images captured from 1973 to 1998 were also produced, for which limited historical data was available in many instances (Kloiber *et al.*, 2002b).

Baban, (1993a) used a combination of remote sensing and GIS to map chl *a* ($r$ = 0.85), suspended solids ($r$ = 0.88) and Secchi depth ($r$ = -0.83) in the Norfolk Broads, England. Mapped suspended solid concentrations were used to analyse water circulation patterns, as they can act as natural tracers indicating the direction of water movement. It was suggested that Geographic information systems (GIS) could take full advantage of the water quality data provided by remote sensing in terms of developing management strategies and testing the individual consequences of any implemented management strategy. Remote sensed information could be combined with hydrological information in a GIS database including information on water quality, depth and flushing rates, land cover, soil type, and locations of point source pollution. Remote sensing also has the ability to provide information on lake catchments such as land use and temporal land use change (Baban, 1999). The thermal Band 6 of Landsat has also been used to study lake thermal regimes. Information relating temperature patterns to lake depth is essential (Baban, 1993b).

Analytical optical modelling to determine water quality has not been widely used using Landsat data due to the low spectral resolution of this sensor. This method is based on sound physical modelling of light through water and its constituents, and the atmosphere. It has previously been used to map suspended solid concentrations using Landsat and Spot data (Dekker *et al*., 2002). These models can be used without *in situ* data, allowing for multi site, multi temporal and multisensor comparisons. Bio-optical models are based on the *in situ* inherent optical properties discussed in chapter one. It has been found that bio-optical algorithms for total suspended solids (TSS) could produce a more reliable multi-temporal algorithm. Also, random point samples for TSS were found to be on average within a mean value of plus or minus 20 to 30% of *in situ* point samples, however in the worst case scenario values were out by 4000% (Dekker *et al*., 2002). The parameter values of the model must be correct otherwise large errors can result in the prediction of water quality parameters (Koponen, 2006).

Table 2.3. Summary of recent remote sensing studies of lake waters using Landsat imagery. (MSS – Multispectral Scanner, TM – Thematic Mapper, Chl – chlorophyll *a*, Sec – Secchi depth, Tur – turbidity, TSS – total suspended solids, SPM – total suspended particulate material).

| Location | Sensor | Variable | Technique | Reference |
|---|---|---|---|---|
| Minnesota | TM, MSS, | Sec,Chl, Tur | B1/B3 ($r^2$=0.85) | Lillesand *et al*. (1983), Kloiber *et* |
| Norfolk Broads | TM | Sec,TSS, Chl | TM3, TM3/TM1 ($r^2$=0.85) | Baban (1993) |
| Lake Erken | TM | SPM, Chl | Chromaticity (green: $r^2$=0.93) | Oestlund *et al*. (2001) |
| Lake Garda | TM | Chl | TM1/TM2, TM1/TM3 ($r^2$=0.72) | Zilioli and Brivio (1996) |
| Frisian Lakes | TM & Spot | Chl | Bio-optical modeling | Dekker *et al*. (2002) |
| Gulf of Finland | TM | Chl , TSS, Sec, | Empirical neural network | Zhang *et al*. (2002) |
| Lake Balaton | TM | Chl | Mixture modeling ($r^2$=0.95) | Tyler *et al*. (2006) |
| Lake Kinneret | TM | Chl | (TM1-TM2)/TM3 | Mayo *et al*. (1995) |

High spectral resolution sensors are available for water quality mapping of large lakes (e.g., MODIS, SeaWiFS and MERIS). These sensors have narrow bands (10

nm) tuned to chl *a* diagnostic signature areas. This allows the formulation of complex bio-optical algorithms for the determination of all optical water quality parameters simultaneously for optically complex inland waters. Significant advances are currently being made in bio-optical modelling of inland waters (e.g., Albert and Mobley, 2003).

When relating point samples to satellite data, areas of interest (AOIs) with depths of at least 3 m or twice the Secchi depth are required for open water signature acquisition. The AOI or sampling frame must contain at least 8 pixels in smaller lakes and up to 1000 pixels in larger lakes (Kloiber *et al.*, 2001a). Large AOIs can have a higher correlation to reference data due to the smoothing of radiometric noise (Lillesand *et al.*, 1983).

## 2.2 Objectives

The objectives of my study were to:

1) Formulate empirical models to predict water quality in all lake pixels using Landsat ETM+ satellite imagery combined with ground data.
2) Apply empirical models to another image for which *in situ* data was unavailable.

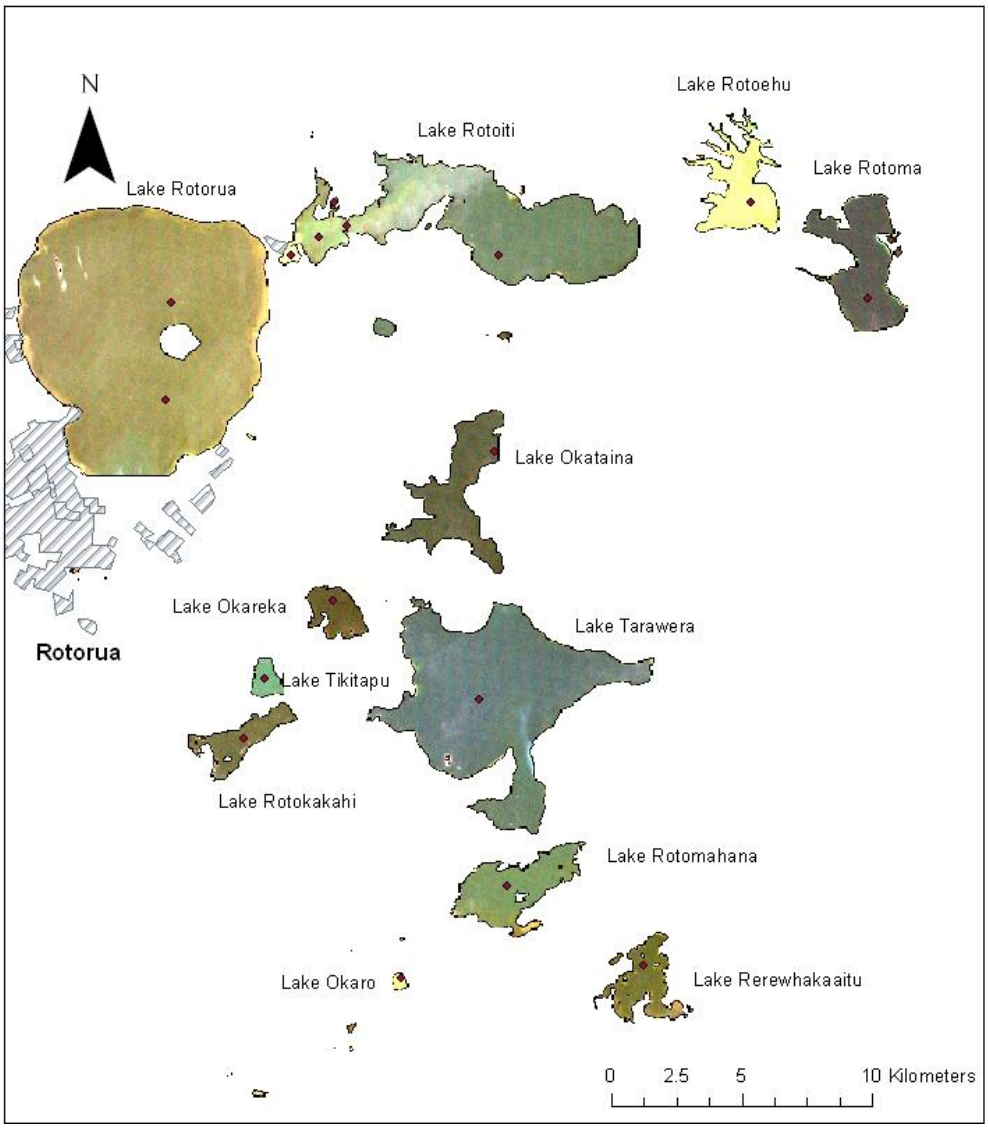


Figure 2.1. True colour composite image (standard deviation stretch) from 25 January 2002 of visible bands 1-3 from Landsat 7 ETM+ including sampling stations.

## 2.3 Study site

We analysed images that showed the 12 main Rotorua lakes (Table 2.4, Figure 2.1). Phosphorus is most often the limiting nutrient to algal growth in freshwater systems, however in the Rotorua lakes, nitrogen has also been shown to be a limiting nutrient (White *et al.*, 1985). More recent studies, however, suggest that with the

predominance of internally regenerated nutrients in Lake Rotorua, phosphorus may be the limiting nutrient in that system (Burger *et al.*, 2007).

Table 2.4. Summary of Rotorua lakes physical characteristics including land cover as percentage of catchment area. Source: Scholes and Bloxham (2007).

| Lake name | Lake area (km²) | Catchment area (km²) | Depth (m) | | Pasture (%) | Indigenous forest/scrub (%) | Exotic forest (%) |
|---|---|---|---|---|---|---|---|
| | | | Maximum | Mean | | | |
| Rotorua | 80.6 | 441.4 | 44.8 | 11.0 | 51.8 | 25.1 | 14.3 |
| Tarawera | 41.3 | 143.1 | 87.5 | 50.0 | 19.7 | 62.4 | 16.0 |
| Rotoiti | 34.0 | 123.7 | 125.0 | 60.0 | 15.9 | 36.4 | 46.2 |
| Rotoma | 11.1 | 27.8 | 83.0 | 36.9 | 23.4 | 46.0 | 26.7 |
| Okataina | 10.8 | 59.8 | 78.5 | 39.4 | 10.7 | 84.1 | 7.8 |
| Rotomahana | 9.0 | 83.3 | 125.0 | 60.0 | 43.2 | 39.7 | 16.3 |
| Rotoehu | 8.0 | 49.2 | 13.5 | 8.2 | 34.2 | 33.4 | 32.0 |
| Rerewhakaaitu | 5.3 | 37.0 | 15.8 | 7.0 | 75.3 | 7.2 | 15.2 |
| Rotokakahi | 4.4 | 19.7 | 32.0 | 17.5 | 26.3 | 16.6 | 57.1 |
| Okareka | 3.4 | 18.7 | 33.5 | 20.0 | 37.8 | 51.6 | 7.6 |
| Tikitapu | 1.5 | 6.2 | 6.2 | 18.0 | 7.0 | 74.3 | 17.9 |
| Okaro | 0.3 | 3.9 | 18.0 | 12.1 | 90.6 | 2.1 | 6.3 |

Many of the Rotorua lake catchments have been converted to exotic forest, farmland or urban areas, which has lead to an increase in phosphorus and nitrogen loading. Management plans are either currently being developed or are in place and are focusing on reducing nutrient inputs through various methods (Scholes and Bloxam, 2007). Internal loading of lakes due to past nutrient inputs and water quality deterioration can take decades to recover. A further problem in addressing eutrophication is that the time lags between nutrient inputs entering groundwater and subsequently entering lakes is considerable, as the mean residence times of water entering Lake Rotorua range from 15-130 years (Morgenstern and Gorden, 2006).

## 2.4 Method

We used ERDAS Imagine for image processing, following the methods of Kloiber *et al*., (2002a). ArcInfo was used for the production of water quality maps and Statistica or Microsoft Excel for statistical analysis.

### *2.4.1 In situ sample collection*

Physiochemical data (Secchi depth, chl *a*, total phosphorus (TP), total nitrogen (TN), and turbidity) for the Rotorua lakes was obtained from Environment Bay of Plenty (EBOP) (Appendix 1A and 1B). Sixteen sampling stations were used in the 25 Jan 2002 regression (including two from Taupo) Most *in situ* samples were collected within 4 days of image capture. The exceptions were Rerewhakaaitu which was collected on the 9 January 2002 and Rotoiti Te Weta Bay which was collected on the 17 of January 2002. Physiochemical data for Lake Taupo was taken from Gibbs (2004). Thirteen sampling stations (including three from Taupo) were used for the 24 October 2002 regression. The Rotorua lakes *in situ* samples were collected within 3 days of the image capture and Lake Taupo *in situ* samples were collected on the 9 October 2002.

### *2.4.2 Image acquisition*

We examined two images covering a 185 km by 185 km area, taken on 25 January 2002 and 24 October 2002. The 25 January 2002 image **(**NASA Landsat Program, 2002, Landsat ETM+ scene path 72, row 86, USGS, Sioux Falls, 25 January 2002)

was pre-processed by Landcare Research New Zealand (resampled to 15 m pixel size, NZMG) for MAF (Ministry of Forest and Agriculture) and subsequently obtained by The University of Waikato Department of Geography. The 24 October 2002 image (NASA Landsat Program, 2002, Landsat ETM+ path 72, row 87, USGS, Sioux Falls, 24 October 2002, Universal Transverse Mercator projection) was acquired free of charge though the GLCF (Global Land Cover Facility) website.

### *2.4.3 Image sampling*

A water-only image was initially created to confine data analysis areas to the lake water surface and to create a base for pixel level classification maps of water quality parameters. Image pixels were initially grouped into ten classes using the isocluster algorithm in ERDAS Imagine, which produced a new thematic coverage. This classification identified statistical patterns in the data and classified the data into ten classes based in the spectral response in bands 1-7 (excluding the thermal Band 6), creating a new coverage or map that was then used as a binary mask to remove terrestrial areas from the image.

Unsupervised classification of the water-only image using ten classes was then undertaken to highlight areas affected by reflectance from aquatic vegetation, shoreline and bottom sediment. These pixels were easily identified as they had elevated brightness in the near infra-red.

The sampling depth of remote sensing instruments depends on the attenuation of light in water. Electromagnetic radiation in the visible spectrum penetrates further

in water with low chl *a*, SS, and DOM. This means that in shallow waters, part of the reflectance signature may be composed of bottom reflectance.

Table 2.5. Environment Bay of Plenty Rotorua lakes sampling site locations (New Zealand Map Grid 1949).

| Lake name | Site | EBOP reference | NZMG easting | NZMG northing |
|---|---|---|---|---|
| Rotoma | 65 m basin | BOP130007 | 2824950 | 6343360 |
| Okataina | 65 m basin | BOP130009 | 2810600 | 6337500 |
| Rotoiti | Site 3 | BOP130005 | 2804940 | 6346190 |
| Rotoiti | Site 4 | BOP130059 | 2810780 | 6345030 |
| Rotoiti | Okawa Bay | BOP130047 | 2802780 | 6345060 |
| Rotoehu | Central main basin | BOP130029 | 2820440 | 6347060 |
| Rotorua | Site 2 | BOP130002 | 2798000 | 6339500 |
| Rotorua | Site 5 | BOP130027 | 2798200 | 6343200 |
| Tarawera | Site 5 (80 m depth) | BOP130030 | 2810000 | 6328000 |
| Okareka | Site 1 (32 m basin) | BOP130013 | 2804400 | 6331800 |
| Tikitapu | 25 m basin | BOP130012 | 2801800 | 6328800 |
| Rotomahana | Site 2 | BOP130060 | 2811080 | 6320840 |
| Rerewhakaaitu | Main lake | BOP130014 | 2816290 | 6317980 |
| Okaro | 18 m basin | BOP130017 | 2806900 | 6317100 |

### *2.4.4 Signature acquisition and regression models*

The mean brightness for each AOI location (Table 2.5) was exported to Excel for regression model formulation (10 by 10 cell AOI). A Pearson correlation matrix between *in situ* water quality variables, and average band brightness values and various band ratios was used to indicate which bands are most suitable for creating regression models. Residual analysis was undertaken for chl *a* regression models to check that residuals were independent and normally distributed. Pixel-level water quality maps were then produced for chl *a* by applying the formulated regression models to each pixel.

## 2.5 Results

### *2.5.1 Correlation of Landsat data to water quality parameters*

There were strong relationships between chl *a* measured in µg $l^{-1}$ and Band 1/Band 3 (B1/B3) ratio for the summer (January) and spring (October) 2002 images (Table 2.6). In both images band ratios usually had the highest correlation to water quality variables. The exception was turbidity, which showed the highest correlation to B3 on 24 October 2002, as has been found in other studies (Lindell *et al*., 1999). Chl *a* showed the highest correlation to B1/B3 on the 25 January 2002, although on 24 October 2002 chl *a* showed the highest correlation to the three band ratio ((B1-B3)/B2). The natural log of Secchi depth, chl *a*, and turbidity showed a higher correlation to band ratios than untransformed data, as might be expected (Kloiber *et al*., 2002a).

Table 2.6. Rotorua lakes correlation matrix between satellite data and *in situ* data for the 25 Jan 2002 image (all correlations were considered significant where $p < 0.05$).

| | Image date | |
|---|---|---|
| Water Quality Parameter | 25/01/2002 | 24/10/2002 |
| | Band : Corr | Band : Corr |
| Total Phosphorus (mg $l^{-1}$) | B1/B3 : -0.833 | B4 : 0.807 |
| Total Nitrogen (mg l-1) | B1/B3 : -0.915 | B1/B3 : -0.754 |
| Chl *a* (µg $l^{-1}$) | B1/B3 : -0.772 | B4 : 0.830 |
| Secchi depth (m) | (B1-B3)/B2 : 0.826 | B1/B3 : 0.869 |
| Turbidity (NTU) | B2 : 0.868 | B3 : 0.915 |
| Ln Secchi | (B1-B3)/B2 : 0.939 | B1/B3 : 0.949 |
| Ln chl *a* | (B1-B3)/B2 : -0.954 | B1/B3 : -0.940 |
| Ln Turbidity | (B1-B3)/B2 : -0.931 | B3 : 0.913 |

### *2.5.2 Regression analysis*

For the summer image (25 January 2002), the regression equation was,

$$\text{Ln chl } a = 14.141\text{-}5.0568 \text{ (B1/B3)} \qquad \text{equation 2.1,}$$

for which $r^2 = 0.91$, $N = 16$, and $P<0.001$ (Figure 2.2).

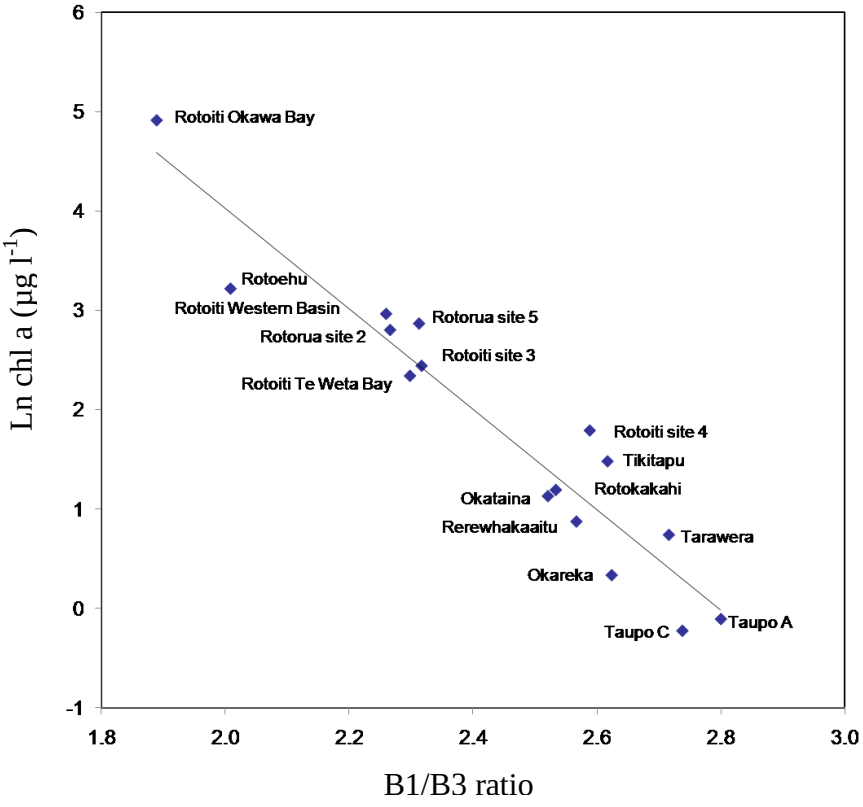


Figure 2.2. Rotorua lakes regression of chlorophyll a concentration in µg l-1 against Band 1/Band 3 from ground data and a Landsat 7 ETM+ image from 25 Jan 2002 corresponding to equation 2.1.

Lake Taupo showed the highest B1/B3 ratio (Figure 2.2), and had the lowest *in situ* chl *a*. Okawa Bay and Lake Rotoiti had the lowest B1/B3 ratio and highest *in situ* chl *a*. Lake Rotoehu had the largest residual (Figure 2.3) in the January image. This could have been caused by the uncertainty of using one point sample to measure the highly heterogeneous chl *a*. The intense algal bloom observed near the sampling

station may mean that chl *a* concentration could undergo rapid temporal fluctuations. Lake Rotoiti site 4 also had high residual values (Figure 2.3).

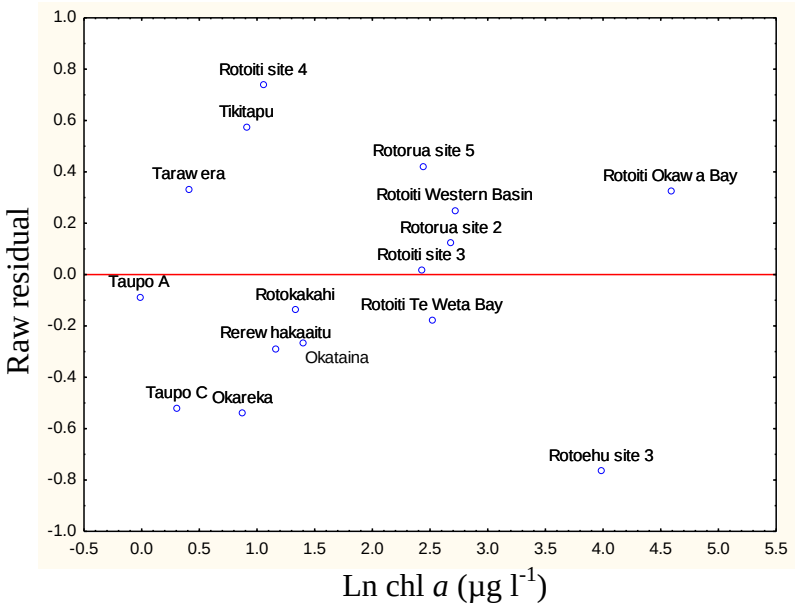


Figure 2.3. Raw residuals vs. predicted values from regression in Figure 4 (equation 2.1).

For the spring image (24 October 2002), the regression equation was,

$$\text{Ln chl } a = 24.251 - 9.2806\ (B1/B3) \qquad \text{equation 2.2,}$$

for which $r^2 = 0.83$, $N = 13$, and $P<0.001$ (Fig. 4). Lake Okaro had the largest residual (Figure 2.5). The *in situ* chl *a* was 89.1 µg $l^{-1}$ here, but the B1/B3 ratio is much lower than expected.

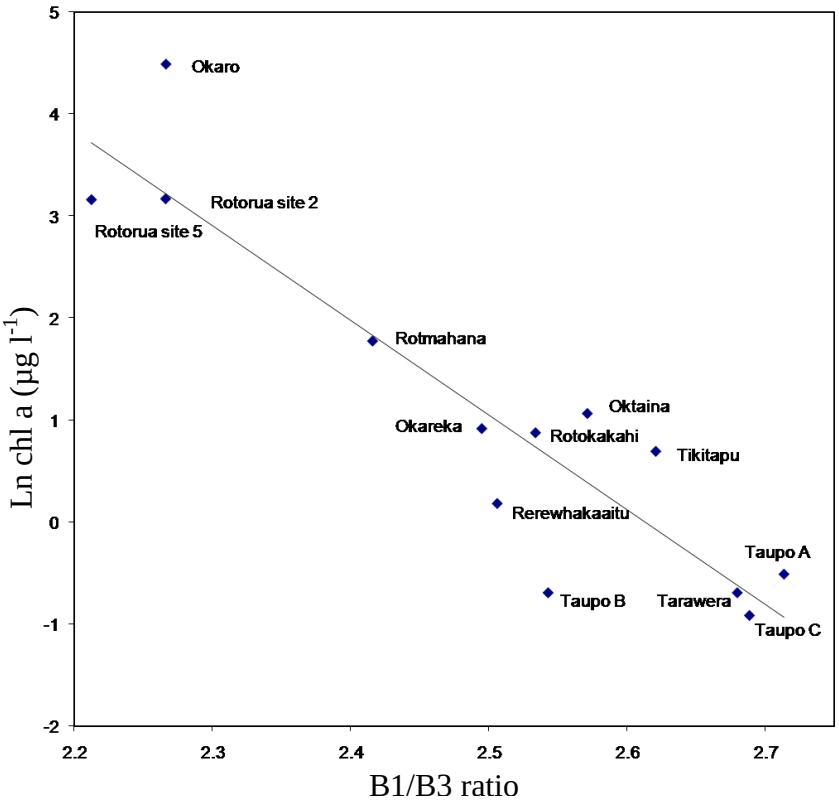


Figure 2.4. Rotorua lakes regression of chl *a* concentration in µg $l^{-1}$ against Band 1/Band 3 from ground data and a Landsat 7 ETM+ image from 24 Oct 2002 corresponding to equation 2.2.

The slopes of the regressions from the 25 January and 24 October 2002 images were significantly different (ANCOVA $P < 0.001$). The two relationships shared the same centroid but had different slopes and intercepts. The difference between the two relationships could have been caused by a number of factors including different processing and resampling levels in the two images, different species of phytoplankton, and atmospheric effects.

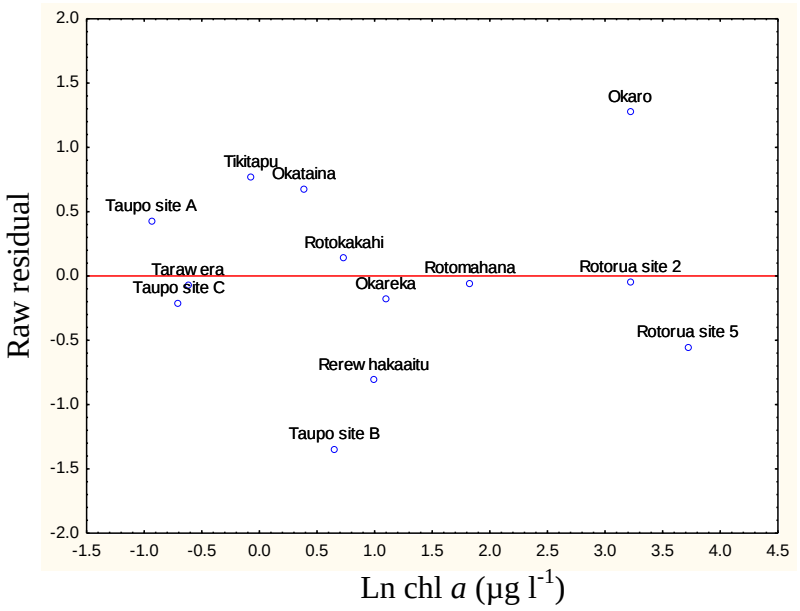


Figure 2.5. Raw residuals vs. predicted values from regression in Figure 2.4 (equation 2.2).

Secchi depth showed a strong relationship with B1/B3 intensity image from the 25 Jan 2002 of the Rotorua lakes (Figure 2.6). Okawa Bay in Lake Rotoiti (western end) had a Secchi depth of 0.78 m whereas in the eastern end Secchi depth was 4.29 m. The regression equation was,

$$\text{Ln SD} = -5.2163 + 2.7753*(B1/B3) \qquad \text{equation 2.3,}$$

for which $r^2 = 0.82$, $N = 14$, and $P<0.001$. The 2002 mean Trophic Lake Index (TLI ) taken from Gibbons-Davies (2003) also showed a strong relationship to the B1/B3 ratio (Figure 2.7), with the regression equation,

$$\text{TLI} = 11.2467 - 3.0985*(B1/B3) \qquad \text{equation 2.4,}$$

for which $r^2 = 0.83$, $N = 10$, and $P = 0.0002$.

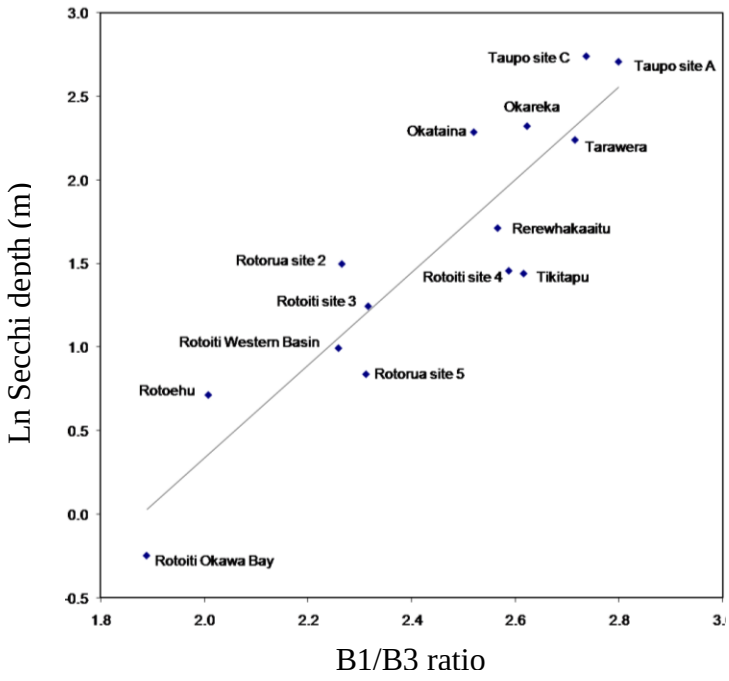


Figure 2.6. Figure 2.6. Regression of Secchi depth in m against Band 1/Band 3 of a Landsat 7 ETM+ image from 25 Jan 2002 of the Rotorua lakes corresponding to equation 2.3.

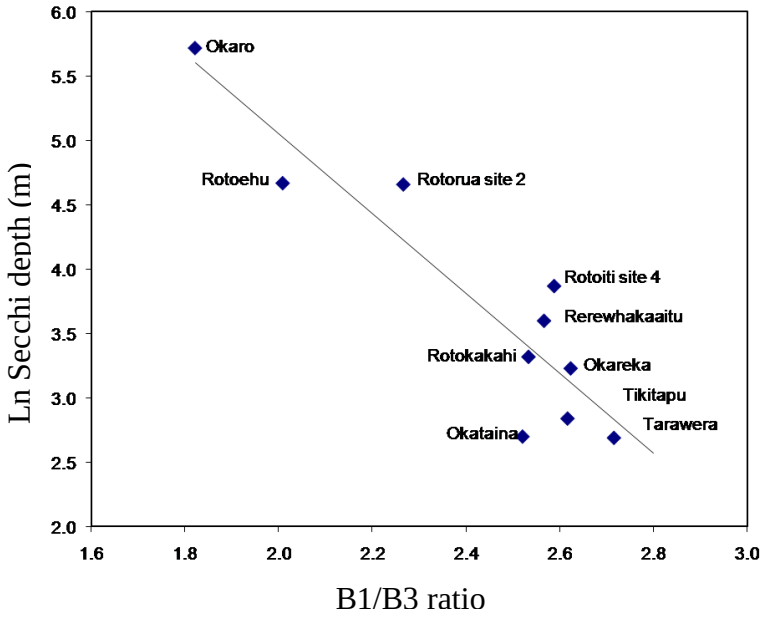


Figure 2.7. Regression between mean 2002 Trophic Lake Index against Band 1/Band 3 from a Landsat 7 ETM+ image from Jan 25 2002 corresponding to equation 2.4.

We also investigated a three band model for the 25 January 2002 Landsat 7 ETM+ image. The regression between measured chl *a* concentration in µg $l^{-1}$ and bands 1, 2, and 3 (B1, B2, B3) was,

$$\text{Ln chl } a = -7.8004*((B1-B3)/B2) + 9.0704 \qquad \text{equation 2.5,}$$

for which $r^2 = 0.91$, $N = 16$, and $P < 0.001$. This three-band model had a slightly higher $r^2$ value than the two-band model (equation 2.1).

### *2.5.3 Chl a concentration maps*

The thematic chl *a* concentration maps produced from regression analysis show significant spatial variation within and between lakes (Figures 2.8-2.18). The highest water quality can be seen in the deep clear lakes of Taupo, Rotoma, Tarawera and Okareka (shown in dark blue). In both images, the effect of reflection from the lake bed near the margins of Lake Rotorua can be seen as elevated erroneous chl *a* predictions, especially on 24 October 2002. On 25 January 2002, chl *a* ranged from 6 µg $l^{-1}$ in the eastern end of Lake Rotoiti (shown in blue) to 136 µg $l^{-1}$ in Okawa Bay (shown in orange/red) (Figure 2.8). This image was captured in late summer, when algal blooms were clearly visible in Okawa Bay, Lake Rotoehu, and Lake Okaro. In the 25 January 2002 image of Okawa Bay it appears that the bloom event was significantly affecting water quality in the western bay area of Lake Rotoiti.

In October, chl *a* was higher in the southern end of Lake Taupo as indicated by the lighter colour (Figure 2.9 and 2.10). Lake Taupo often exhibits a winter surface

chl *a* maximum. Lake Rotorua also showed a relatively high chl *a* concentration (23 µg $l^{-1}$) for winter (Fig. 2.10). A close-up of Figure 2.9 shows the chl *a* distribution in the Rotorua lakes (Figure 2.10).

Using equation 1.1, we predicted chl *a* distribution in an earlier image from summer (5 January 2001; Figures 2.11 and 2.12). Lake Rotoehu and Okawa Bay, Lake Rotoiti, again show high chl *a* concentrations (Figure 2.12). On the 6 January 2001 image, high concentrations of chl *a* occurred in the central west of Lake Rotoehu, in contrast to spatial variability in 2002 (Figure 2.12). Light westerly winds (5.5 km $h^{-1}$) were recorded near the time of this image capture, but do not seem to have had a visible effect on the concentration patterns.

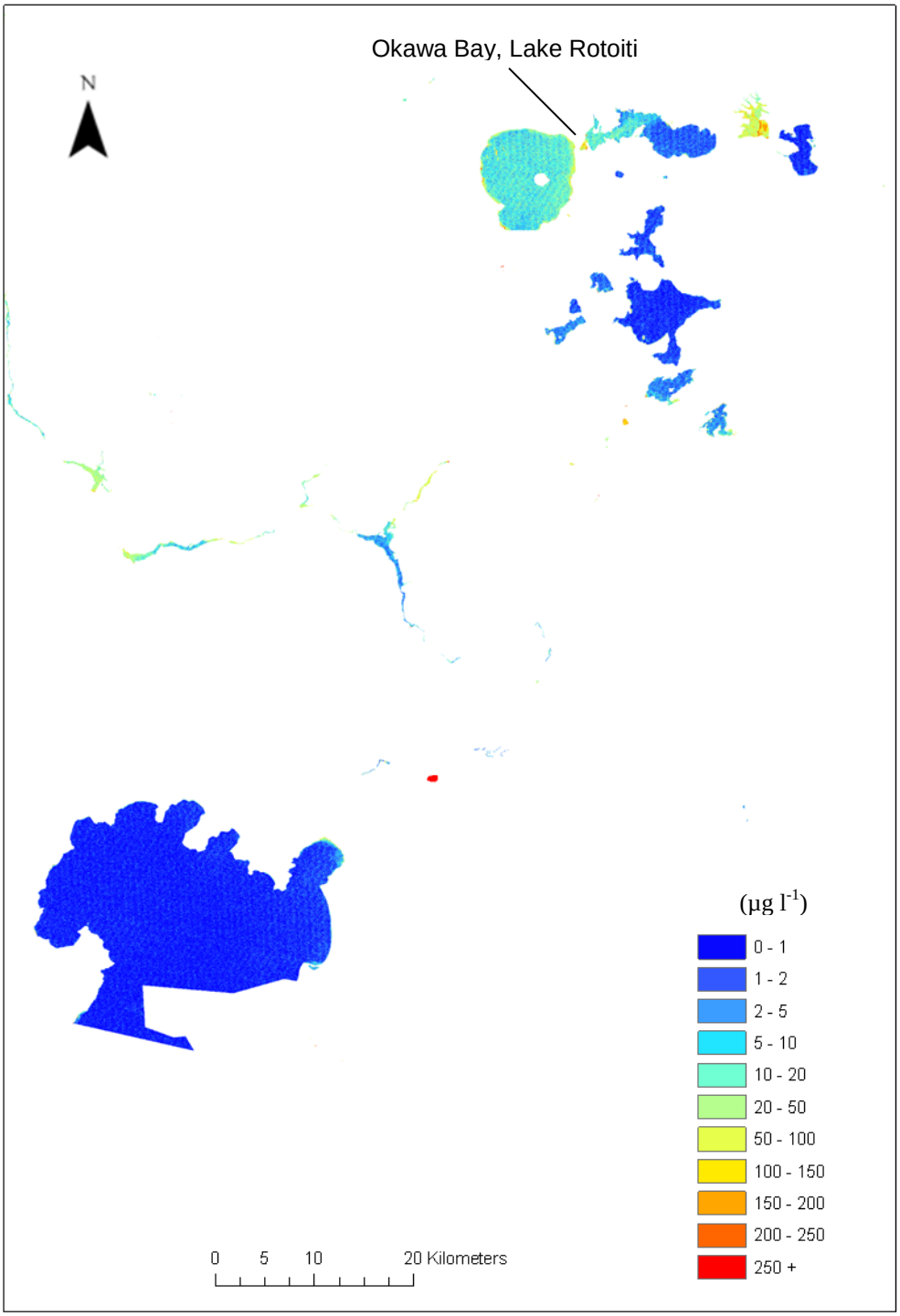


Figure 2.8. Chl *a* concentrations in µg $l^{-1}$ in the Rotorua lakes and Lake Taupo on 25 January 2002 predicted from equation 2.1.

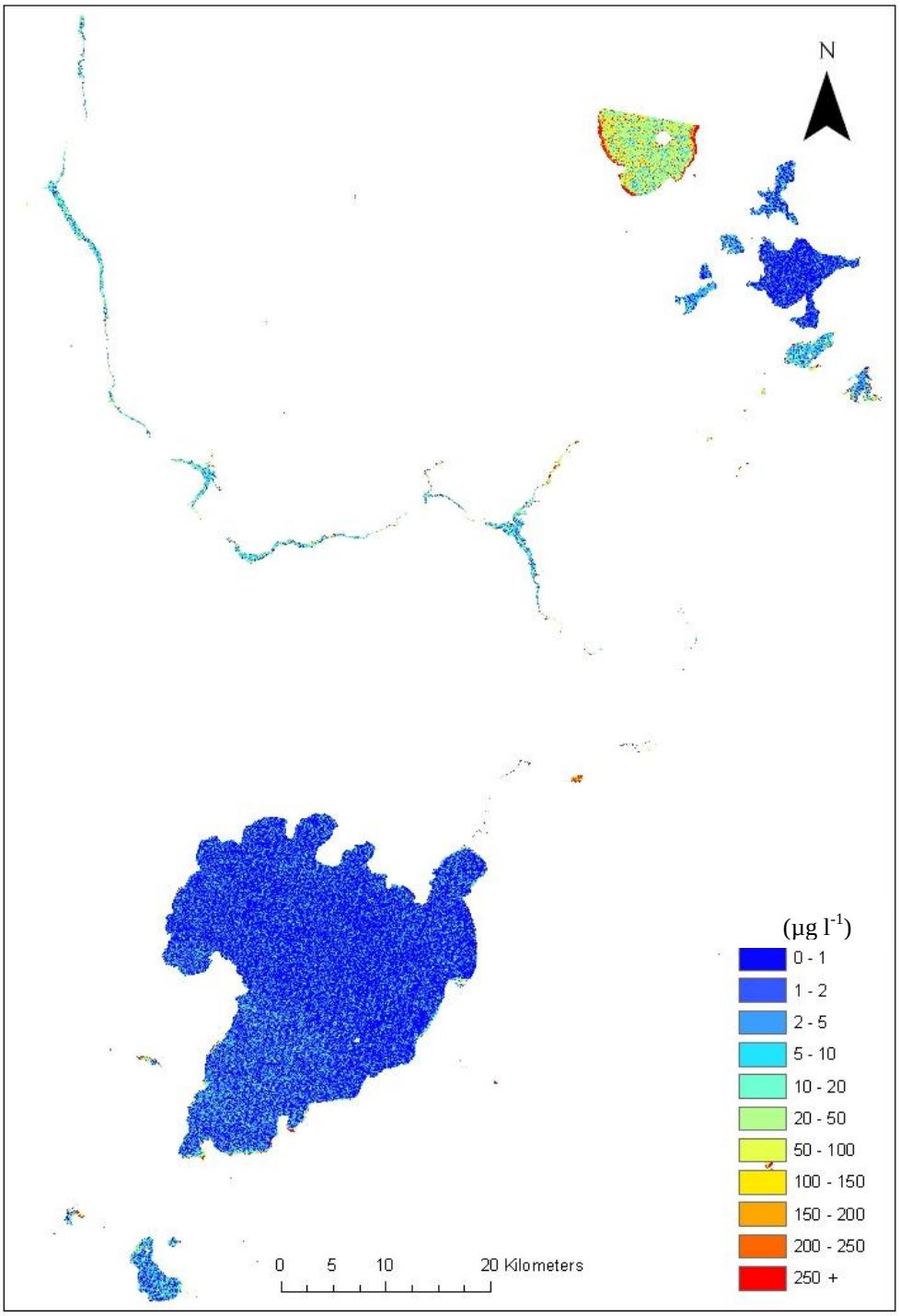


Figure 2.9. Chl *a* concentrations in µg $l^{-1}$ in the Rotorua lakes and Lake Taupo on 24 October 2002 predicted from equation 2.2.

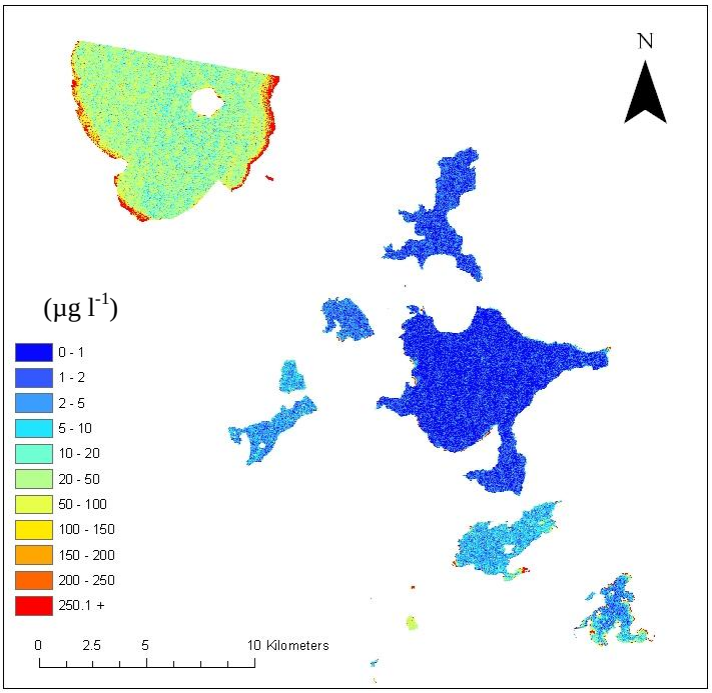


Figure 2.10. Chl *a* concentrations in the Rotorua lakes on 24 October 2002 predicted from equation 2.2.

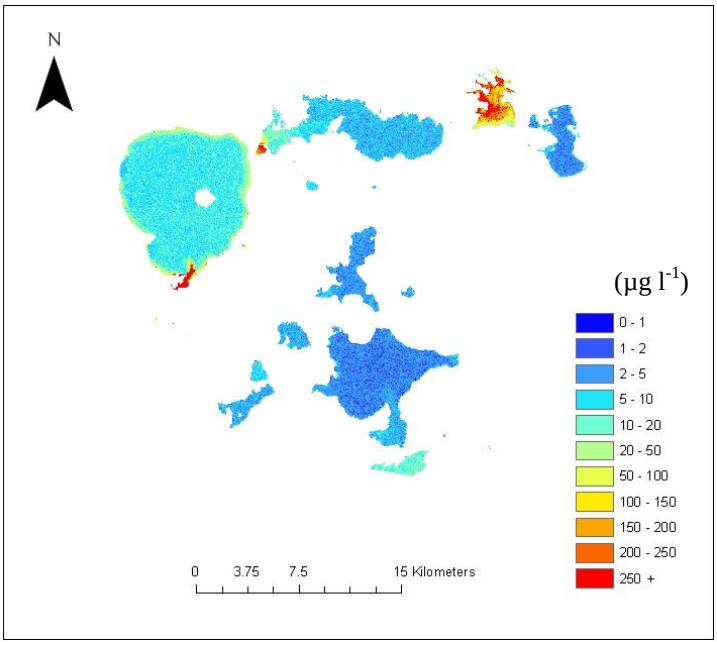


Figure 2.11. Chl *a* concentrations in the Rotorua lakes on 6 January 2001 predicted from equation 2.1.

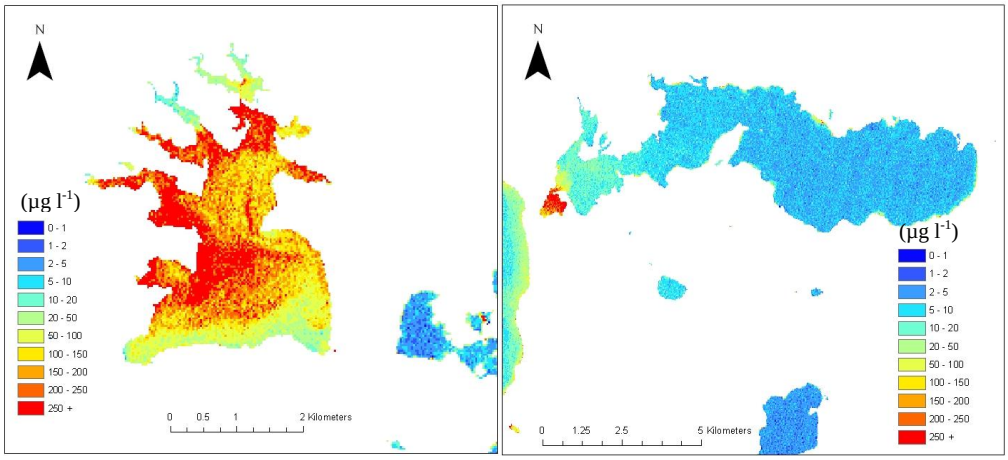


Figure 2.12. Chl *a* concentrations in lakes Rotoehu (left) and Rotoiti (right) on 6 January 2001 predicted from equation 2.1.

## 2.6 Discussion

This work has demonstrated that remote sensing for water quality using traditional band ratio methods is possible for the Rotorua lakes. The accuracy of the chl *a* and Secchi depth retrieval models are comparable with previous studies (see Table 2.3). The chl *a* concentration maps produced from the regression provided insights into the spatial dynamics of phytoplankton blooms. The high correlation found in the semi-log regression relationships between water quality parameters and B1/B3 ratios confirms the results found in previous investigations that band ratios provide useful relationships (e.g., Lilliesand and Johnson, 1983; Mayo *et al*., 1995; Zilioli and Brivio; 1996, Kloiber *et al*., 2002b).

The empirical band ratio method is the most commonly used method for retrieving water quality using remote sensing and it has been shown to be effective in the retrieval of many water quality parameters (see table 2.3). It has been found that the ratio of two bands reduces the effects of factors such as measurement geometry

and atmosphere on the retrieval of water quality (Koponen, 2006). A semi-log regression has also been used in most other inland water quality band ratios. This model has been found to meet the basic assumptions of the technique in respect to residuals having constant variance, independence and being normally distributed (Kloiber *et al.*, 2002a).

When comparing the results obtained from two and three band ratios, the B1/B3 ratio usually provided the highest correlation (Table 2.6). The three band ratio was also used by Mayo *et al*. (1995) ($r^2$=0.80). Since the two band ratio showed more consistent correlation to *in situ* measurements, and has been more widely used, it was decided to use this ratio to predict water quality.

Generally, the resulting regression equation coefficients have atmospheric and specific lake scene factors imbedded (Kloiber, *et al*., 2002a). This means that these equations are specific to this scene and the prediction of the 5 January 2001 image should only be interpreted as a general guide to the bloom distributions at this time. Despite uncertainties involved in quantitative analysis of water quality with satellite imagery, the results still provide a valuable snapshot of spatial variation in phytoplankton blooms in lakes Rotoehu and Rotoiti.

Although the spectral bands Landsat ETM are broad enough to encompass a mixture of spectrally opposing absorption and scattering features (Dekker *et al*., 1992), we were still able to develop relationships between Landsat bands and water quality variables. Band 3 encompasses the chl *a* absorption minimum as well as a significant part of the scattering peaks on either side of this minimum. Although these are contradictory features the net effect is that as water clarity decreases brightness in bands 2-4 increases (Kloiber *et al*., 2002a). The underlying physical

basis for this result has been studied by several investigators (eg. Han, 1997; Bukata *et al.,* 1995).

Algal blooms often consist of rapid rises in cell numbers followed by a collapse as nutrients and light become limiting. In addition, buoyancy variations, compounded with diurnal stratification, can cause rapid changes in chl *a* concentrations (e.g., Oliver and Ganf 2000). In Lake Rotorua, for instance, many blooms are transient and are not necessarily followed by a collapse. Often they are simply an interaction of large cyanobacterial biomass combined with diurnal stratification of the surface mixed layer, allowing the positively buoyant cells to congregate at the water surface; this is often disrupted on a daily basis, e.g., by an afternoon wind. These time scales mean that the timing of image collection should be carefully recorded and assessed with regard to potential for this surface aggregation process (D. P. Hamilton, pers. comm.). Time difference between *in situ* sample collection and satellite image acquisition is a potential source of error in this study.

TLI is an index composed of chl *a*, Secchi depth, TP concentration, and TN concentration, so it is not surprising that a strong relationship exists between it and the B1/B3 ratio as all of these factors have the potential to affect water colour and clarity and are interrelated (Burns *et al.,* 1999).

The main reasons for the increase in incidence of severe algal blooms in Okawa Bay are the shallow sheltered nature of the bay and possibly the input of nutrients through the lake bed or from septic tank leakage. Quantitative information on water quality in Okawa Bay was not available before 1997 (Ray *et al.,* 2002). Remote sensing may be able to address this lack of data through retrospective analysis of past Landsat images.

Spatial variation in lakes with high productivity can be large, meaning traditional point sampling methods can misrepresent the general lake condition (Dekker *et al*., 2002). Using a single monitoring station can over or underestimate chl *a* by 29 – 34% (Kallio *et al.*, 2003). The areas of higher concentration (red colour) provide possible insights into the hydrodynamics of Lake Rotoehu as this area corresponds to a change in bathymetry to deeper areas to the west. Strong northwest winds (about 30 km $h^{-1}$) were recorded on the day of image capture which may be responsible for the higher concentration in the southeast of Lake Rotoehu.

Analysis of Landsat imagery has the advantage of having the longest continuous high resolution satellite data set, with the first Landsat MSS images taken in 1972. Temporal analysis of water quality trends could provide information on long term water quality trends, in spatial context. The Landsat Data Continuity Mission (LDCM) satellite is expected to be launched in 2011 ensuring the continuation of this long running data set.

Limitations to monitoring water quality with Landsat data include, the low temporal resolution which limits the utility in studies of dynamic processes. Clear weather is needed on satellite overpass dates, which can mean some data is not suitable for use due to cloud cover. With the launch of numerous other satellites with comparable features to Landsat (such as ALOS and ASTER), the temporal resolution of image capture will be increased.

Lakes characterized by high suspended sediment can often pose a problem as TSS can dominate spectral reflectance. Sub-pixel analysis may provide a solution to these problems, as the signatures of chl *a* and SS could be unmixed.

If unprocessed images are purchased, digital numbers can be converted to at-satellite reflectance (which accounts for voltage bias and gain of the sensor, varying sun angle, and variation in Earth Sun distance). Subsequently, more confidence can be placed in atmospheric correction or image to image normalisation. A scene shift could be applied to these images which would encompass all of the Rotorua lakes and all of Lake Taupo in one image.

Two recent Landsat 5 images from summer 2005 and spring 2006 exist with *in situ* Biofish data (taken within 2 days of image capture). The Biofish provides a lateral 'snapshot' (depth and transect distance) of chl *a*, which would enable analysis of water quality in 3 dimensions. If all images are processed from raw data using standard reflectance conversion and atmospheric correction techniques, a more direct comparison between images from Landsat 5 TM and Landsat 7 ETM+ will be possible.

## 2.7 Conclusions

Remote sensing provides synoptic predictions of water quality, which can aid our understanding of the patterns in spatial variation of water quality and its causes. When high within lake variation of chl *a* occurs, remote sensing can increase the accuracy of synoptic monitoring when combined with ground observations, by providing information on spatial variation.

The high correlation between B1/B3 and *in situ* chl *a* found in both January and October 2002 means that chl *a* can be mapped when image and *in situ* data are present. Improvements in satellite data quality (processing level) and atmospheric

correction could increase the temporal stability of the relationship meaning that it may be possible to create a standard model which can be applied to predict chl *a* concentration in images that do not have corresponding ground data.

High correlation between B1/B3 and Secchi depth means that pixel level water quality maps can also be created for this parameter. TLI also shows a strong relationship to B1/B3. TLI is based on the water quality parameters TN, TP, Secchi and chl *a* therefore it is not surprising that this relationship occurs. Pixel level maps of TLI may provide lake managers with a useful guide to pinpoint problem areas within individual lakes, such as Okawa Bay in Lake Rotoiti.

Chl *a* pixel-by-pixel concentration maps provide insight into spatial variability and can lead to an increase in the accuracy of monitoring in lakes with high spatial variation such as Rotoehu and Rotoiti. Monitoring of these lakes may need to include mean chl *a* in the monitoring regime. On 25 January 2002, intense algal blooms occurred and complex spatial variation in phytoplankton density can be seen in lakes Rotoiti and Rotoehu. The 6 January 2001 image also showed large spatial variation in water quality in these lakes but with a different pattern occurring in Lake Rotoehu, where higher concentrations of chl *a* are seen in the central west area of the lake rather than in the southeast.

# 3. Waikato lakes

## 3.1 Introduction

Monitoring of lakes using traditional point sampling methods is expensive while often not effectively monitoring spatial variation of water quality variables (Dekker *et al*., 2002). While high-spectral resolution ocean colour monitoring platforms have been designed to effectively monitor water quality, their coarse spatial resolution limits their application to the largest lakes. Therefore, the choice of platforms for smaller lakes is limited to higher spatial resolution platforms such as Landsat, which usually have lower spectral resolution (Tyler *et al.,* 2006).

In deep lakes, relationships between chl *a* and remote sensing reflectance are relatively simple due to the low concentrations of suspended sediment (SS), and can be derived from traditional band ratio methods as chlorophyll (chl) *a* is the primary colour producing agent (e.g., Lilliesand and Johnson, 1983, Zilioli and Brivio, 1996). However when high and heterogeneous concentrations of SS are present, chl *a* concentrations are more difficult to derive from coarse spectral resolution satellites (Lindell *et al*., 1999).

Linear spectral unmixing to determine water quality is still a relatively new technique. Svab *et al*., (2005) used controlled tank experiments and *in situ* spectroradiometry of simulated Landsat reflectance to variations in SS and chl *a*. Principal components analysis (PCA) of the simulated reflectance showed that turbid lake water possesses spectrally unique endmembers.

Tyler *et al*. (2006) applied the spectral mixture modelling approach to Lake Balaton, which is Europe's largest freshwater lake by surface area. Lake Balaton has a mean depth of 3 m, and is characterised by heterogeneous distributions of TSS (3 – 300 mg $l^{-1}$) and chl *a* maximums of 240 µg $l^{-1}$. High correspondence between *in situ* measurements of chl *a* and modeled image derived chl *a* was achieved, while yielding considerable detail of lake phytoplankton distribution ($r^2 = 0.95$). This calibration was the successfully applied in retrospective analysis of a 1994 image, validated with chl *a* data coincidentally collected within two days of image capture. This calibration was demonstrated to be robust and have temporal stability.

Thiemann and Kaufmann (2000) used Indian Remote Sensing Satellite (IRS-1C) imagery to investigate a linear spectral unmixing model to estimate chl *a* in lakes in Mecklenburg, Germany ($r^2 = 0.85$). In contrast to other studies, only two endmembers, chl *a* and clear water were used to unmix the data, as SS and dissolved organic matter (DOM) levels were low enough to be neglected. This method was found to be more accurate when compared estimates of chl *a* obtained from Band 3, and Band 4/Band 3 ratios.

Rudorff *et al*. (2006) investigated linear spectral unmixing of Hyperion hyperspectral data of Amazon floodplains, Brazil, using four endmembers, including phytoplankton, SS, DOM and clear water. These authors concluded that nonlinear mixing of optically active components can result in a fraction image of 0 % or 100 %, which can indicate negative estimates or over 100 % estimates of the endmember. A low positive correlation was found ($r = 0.52$) between the unmixed chl *a* abundance image and *in situ* data. Suspended mineral concentration showed a non-linear

relationship to the SS endmember abundance image ($r$ = 0.75). No significant correlation to DOM was found.

Due to the persistent nature of cloud cover in the Waikato region and time/ financial limitations, it was decided that retrospective analysis of past satellite images would be a good option to test the feasibility of linear spectral unmixing in the Waikato region. This investigation used a mixture modelling approach using two freely available Landsat 7 ETM+ images with *in situ* samples coincidentally taken within three days of image capture.

## 3.2 Study site

This study covers lakes of the northern Waikato region which includes more than 40 lakes ranging from 0.01 km² to 34.4 km² in area (Figure 3.1). There are 31 dystrophic (peat) lakes in the Waikato region, which are a remnant of the formerly extensive peat bogs of Komakorau, Rukuhia and Moanatuatua, forming the largest peat habitat in New Zealand. Peat lakes have classically been described as having low productivity, however, recent more detailed investigations have shown that chl *a* is significantly higher in coloured lakes than clear lakes. Also, annual integral productivity of epilimnetic bacterioplankton has also been found to be much higher in peat lakes than in clear water lakes (Nurinberg and Shaw, 1998). An Anoxic hypolimnia is common in peat lakes due to decomposition of organic carbon (Wetzel, 2001). Peat lakes are typically brownish due to high levels of DOM leached from surrounding peat lands, and are generally mildly acidic (pH 5.5 – 6.5). In this study,

*in situ* data was collected for peat lakes Serpentine North, Rotomanuka North and South, Ngaroto, Maratoto and Rotokauri.

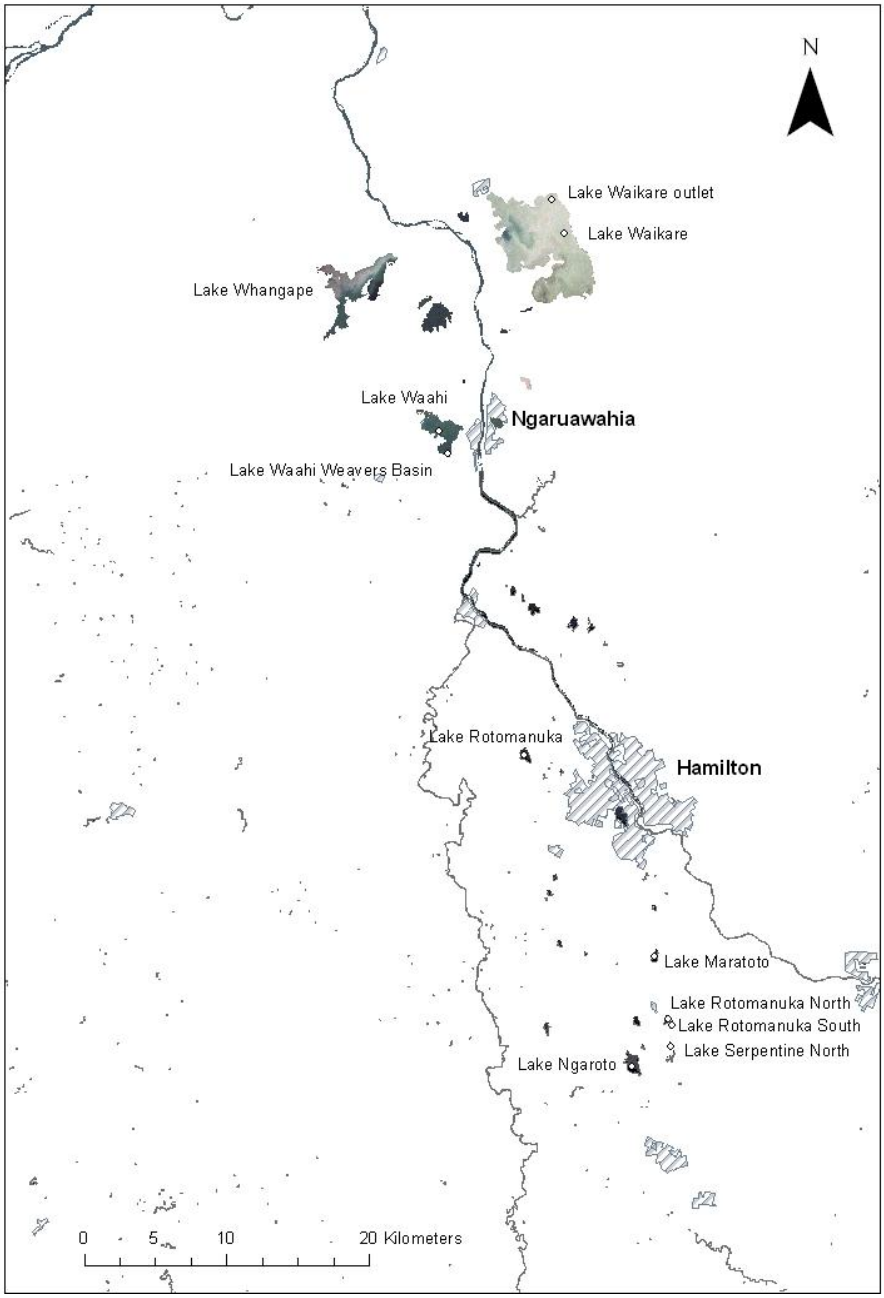


Figure 3.1. Waikato study site map including lakes and sampling stations (open circles). Lakes are a true colour composite of Landsat bands 1-3 from 28 August 2002 (with a standard deviation colour stretch).

The larger riverine lakes sampled in this study include lakes Waikare and Waahi, which were formed when alluvial deposits diverted the original path of the Waikato River, damming valleys and tributaries.

Lake Waikare is a large shallow hyper-eutrophic lake characterized by extremely high levels of inorganic suspended sediment. This sediment can be attributed to erosion from the Matahuru catchment and from resuspension from the lake bed by wave action. The high SS concentrations found here are thought to be the principal factor controlling productivity in the lake, limiting light penetration and hence phytoplankton growth (Barnes , 2002). The SS in Lake Waikare consists mainly of clay particles which are easily resuspended, keeping the lake in a constant turbid state even during periods of stable weather (Reeves *et al*.; 2002, Stephens *et al*., 2003).

Lake Whangape is the second largest lake in the Waikato region. It is a shallow hyper-eutrophic lake with an average depth of 1.5 m. During summer the lake has weak thermal stratification with oxygen depletion in deeper waters (Boswell *et. al*., 1985). The lake catchment is consisted of mainly agricultural land, but in the past the lake has received inputs from mining activities (Barnes, 2002). This lake suffered a *Egeria densa* macropyte collapse in 1987 (Champion et al., 1993). This has been attributed to a number of factors including phytoplankton blooms, grazing from pest fish, cultural eutrophication, and increase in inorganic sediment levels (Wells *et al*., 1988). Vant (1987) attributed the macropyte collapse to discharge of inorganic sediment in mining waste water.

Lake Waahi is a relatively shallow super-eutrophic lake dominated by high turbidity and high algal biomass. Current monitoring programs indicate that the lakes

water quality has stabilized since the macrophyte collapse in the late 1970s, which was attributed to low lake levels, high nutrient concentrations, and continued sediment input from mining (Dell *et al.*, 1998).

Lake Rotomanuka North is a small eutrophic peat lake remnant of the once larger Lake Rotomanuka, the past lake bed forming the surrounding wetland (10 ha) that connects to Lake Gin (Rotomanuka South). The catchment is comprised of intensive dairy and pastoral farming. Analysis of water quality samples collected between October 1995 and December 2001 shows a probable degradation of water quality over time, with a percent annual change of $6.5 \pm 3.5$ %.yr$^{-1}$ ($p = 0$ 0.15). The decrease in water clarity, increase in total nitrogen and total phosphorus could be attributed to the collapse of macrophyte beds that occurred in 1996/1997, where the input of detritus and following microbial decomposition nutrients released organic nitrogen and phosphorus, which for some reason remains unavailable (Barnes, 2002). Furthermore, little seasonality was observed in water quality parameters (Barnes, 2002) although stratification and bottom anoxia has been recorded in summer months (Boswell *et al*., 1985).

## 3.3 Methods

### *3.3.1 In situ sample collection*

Seven *in situ* samples were taken by EW (Environment Waikato), over six lakes (six chl *a* samples and seven turbidity and TSS samples) on the 28 and 29 March 2000, which coincided with a Landsat ETM+ overpass on the 31 March 2000. Also, seven *in situ* samples were taken by EW, over five lakes (six chl *a* samples and seven

turbidity and TSS samples) on the 27 and 28 August 2002, which coincided with a Landsat ETM+ overpass on the 28 August 2002. EW sampling locations were converted from NZMG (New Zealand Map Grid) coordinates to the UTM (Universal transverse Mercator) map projection zone 61S.

Specific details regarding EW water quality sampling and laboratory analysis can be found in Appendix 4. Surface water chl *a* and nutrient of a known volume were filtered, and chl *a* measured using acetone extraction and spectroscopy. Suspended solids were sampled directly and dried at 104ºC. Volatile suspended solids were filtered using pre-combusted glass fiber filters (Whatman GF\C) and ashed at 550ºC.

### *3.3.2 Image data*

This study used two freely available Global Landcover Facility (GLCF) Landsat ETM+ images captured on the 28th August 2002 and the 31 March 2000. The metadata for these images states that the processing level is L1G, indicating that the data has been radiometrically corrected and orthorectified (UTM zone 61S). All subsequent image processing for mixture modelling was carried out on non atmospherically corrected data, but the TSS regression used reflectance values. Furthermore, it should be noted that these images may have been modified by spectral feathering and radiometric adjustments used to generate GLCF mosaics.

In larger lakes, satellite data was sampled by taking the mean reflectance from a 5 by 5 pixel window (142.5 m by 142.5 m) in order to decrease radiometric noise and account for uncertainties in the location of *in situ* data collection. In the small

lakes Maratoto and Serpentine North, a 3 by 3 pixel window (85.5 m by 85.5 m) was used.

### *3.3.3 Conversion to reflectance and atmospheric correction for TSS regression*

Traditional methods used to derive TSS concentration maps used reflectance values calculated incorporating dark object subtraction atmospheric correction (Chavez, 1996). This method has been found to provide a reasonable atmospheric correction for cloud-free scenes (Hadjimitsis *et al*., 2004). Conversion from Landsat L1G scaled radiance to 32-bit radiance (watts per square meter per steradian per micrometer) is the first step and is given by

$$L_\lambda = ((LMAX_\lambda - LMIN_\lambda)/(QCALMAX-QCALMIN)) * (QCAL-QCALMIN) + LMIN_\lambda \quad \text{Equation 3.1,}$$

where:

$L_\lambda$ = Spectral Radiance at the sensor aperture in W $m^{-2}$ $sr^{-1}$ $\mu m^{-1}$

QCAL = the quantized calibrated pixel value in digital number

$LMIN_\lambda$ = the spectral radiance that is scaled to QCALMIN in W $m^{-2}$ $sr^{-1}$ $\mu m^{-1}$

$LMAX_\lambda$ = the spectral radiance that is scaled to QCALMAX in W $m^{-2}$ $sr^{-1}$ $\mu m^{-1}$

QCALMIN = the minimum quantized calibrated pixel value (corresponding to $LMIN_\lambda$) in digital number

= 1 (LPGS Products)

= 0 (NLAPS Products)

QCALMAX = the maximum quantized calibrated pixel value (corresponding to $LMAX_\lambda$) in DN

= 255

Dark object subtraction assumes that somewhere in the image there should be a target with a true value of zero having zero reflection. When the image histogram is analysed, the minimum value is taken as an estimate of path radiance, and therefore subtraction of this value from the at-satellite radiance gives an approximation of water leaving radiance. Atmospheric correction procedures are sometimes problematic when working on inland waters with high spatial resolution and low spectral resolution platforms such as Landsat. This can contribute to uncertainties when undertaking a comparison of images taken at different time periods (Hadjimitsis *et al*., 2004). Reflectance is then calculated using the following equation,

$$P_p = \frac{\Pi \bullet L_\lambda \bullet d^2}{ESUN_\lambda \bullet \cos\theta_s}$$ equation 3.2,

Where:

$P_p$ = Unitless planetary reflectance

$L_\lambda$ = Spectral radiance at the sensor's aperture

$d$ = Earth-Sun distance in astronomical units (taken from appendix _)

$ESUN_{\lambda}$ = Mean solar exoatmospheric irradiance (taken from appendix )

$\theta_s$ = Solar zenith angle in degrees (calculated from image metadata (90º- solar elevation angle))

### *3.3.4 Image analysis*

3.4.4.1 Linear Spectral Unmixing (LSU)

Spectral unmixing (Smith *et al.,* 1985) is an inversion technique that aims at estimating the mixture components responsible for the mixed spectral signature of a pixel, defined as a linear-matrix equation:

$$R_i = \sum_{k=n}^{n} f_k R_{ik} + \varepsilon_i \qquad \text{equation 3.3,}$$

where $R_i$ is the reflectance of the mixed pixel for each band *i*, including one or more endmembers; $f_k$ is the fraction of each endmember *k* within the pixel, $R_{ik}$ is the reflectance of the endmember *k* within the pixel on band *i*, and $\varepsilon_i$ is the error for band *i* (or the difference between the measured and modeled DN in each band).

To solve these equations, the endmembers must be independent from each other, the number of endmembers should be less than or equal to the number of spectral bands used, and the spectral bands used should not be highly correlated.

The water surface reflection received by satellites is a mixed spectrum as it is affected by chl *a*, SS, DOM concentrations, as well as other factors. LSU attempts to unmix this signature, deriving proportion estimates of the mixture components. These mixture components are referred to as endmembers, which are idealized pure signatures. In this study, an image based endmember selection process was used where bands are plotted in feature space, and endmembers identified manually using a similar approach to Tyler *et al*., (2006). Spectrally pure endmembers are found at the vertices of the polygon bounding the data cloud in feature space (Smith *et al.,* 1985). ERDAS Imagine was used to geo-link feature space plots so the pixel within the image can be located in feature space. All LSU was carried out on raw data and principal components transformed data.

#### 3.4.4.2 Principal Components Analysis

PCA is performed on six Landsat bands (excluding thermal and panchromatic bands) using ERDAS Imagine. Adjacent bands in multispectral imagery are generally correlated (Mather 2005), which can cause problems when try to unmix the spectral signatures of water quality variables. Only spectrally unique endmembers can be properly evaluated in the unmixing process, as correlation between endmembers can result in negative abundance estimates (Van der Meer and De Jong, 2000). PCA analysis is also used to determine the spectral dimensionality of the data set, with the number of coherent PCA bands representing the number of coherent dimensions. This provides an estimate of the number of spectral endmembers that can be unmixed (Tyler *et al*., 2006). Global analysis of the Landsat ETM+ mixing space has shown that >98% of image spectral variance can be encompassed within a three dimensional mixing space (Small, 2004).

### *3.3.5 Calibration*

Finally, the unmixed fraction images produced by unmixing are regressed against *in situ* water quality samples. The final regression model is then applied to abundance estimates to create thematic water quality maps of TSS and chl *a* concentration.

## 3.4 Results

### *3.4.1 Correlation between Landsat ETM+ reflectance and in situ samples*

Consistent high correlation was found between TSS and reflectance in bands 3 and 4 (Table 3.1), although a subsequent regression analysis was performed on Band 3, as this is the most common band used to map TSS. Chl *a* showed a high correlation to Band 3 in the 2002 image, although there is high covariance between chl *a* and TSS ($r$ = 0.99). However no significant correlation for chl *a* was found in the March 2000 image. TP showed the highest correlation of the nutrient parameters, and also showed very high covariance with TSS ($r$ = 1.0).

Table 3.1. Landsat reflectance data correlation with the most significant relationships for each water quality variable (results in the format of band: correlation: P-value, with significant correlations in bold).

| | Image date | | |
|---|---|---|---|
| Water quality variable | 28/08/2002 | 31/03/2000 | Combined Data |
| Chl *a* (µg $l^{-1}$) | **B3: 0.978: 0.001** | B5: 0.501: 0.252 | **B3: 0.858: 0.000** |
| Volatile suspended solids (VSS) (mg $l^{-1}$) | **B4: 0.984: 0.000** | **B4: 0.820: 0.024** | **B4: 0.813: 0.001** |
| Total suspended solids (TSS) (mg $l^{-1}$) | **B4: 0.987: 0.000** | **B4: 0.998: 0.000** | **B3: 0.980: 0.000** |
| Turbidity (NTU) | **B4: 0.991: 0.000** | **B4: 0.997: 0.000** | **B3: 0.982: 0.000** |
| Dissolved reactive Phosphorus (mg $l^{-1}$) | B5: -0.325: 0.529 | B4: -0.374: 0.409 | B4: -0.356: 0.232 |
| Total Phosphorus (TP) (mg $l^{-1}$) | **B4: 0.993: 0.000** | **B4: 0.915: 0.004** | **B4: 0.876: 0.000** |
| Nitrate + Nitrite (NNN) (mg $l^{-1}$) | B4: -0.684: 0.134 | B4: -.0455: 0.306 | B4: -0.390: 0.188 |
| Total Kjeildal Nitrogen (TKN) (mg $l^{-1}$) | **B4: 0.967: 0.002** | B5: 0.340: 0.456 | B4: 0.274: 0.365 |
| Ammoniacal Nirtogen (mg $l^{-1}$) | B7: -0.682: 0.136 | **B7: 0.798: 0.031** | B4: -0.340: 0.256 |

### *3.4.2 Regression analysis for SS*

Reflectance in Band 3 was used in the final regression equation to predict TSS (Figure 3.2). This relationship was used to create TSS concentration maps. The combined regression equation from both images was

$$TSS = 0.0388 + 0.0008\ (B3) \qquad \text{equation 3.4,}$$

for which $r^2 = 0.98$, $N = 15$ and $p = < 0.001$.

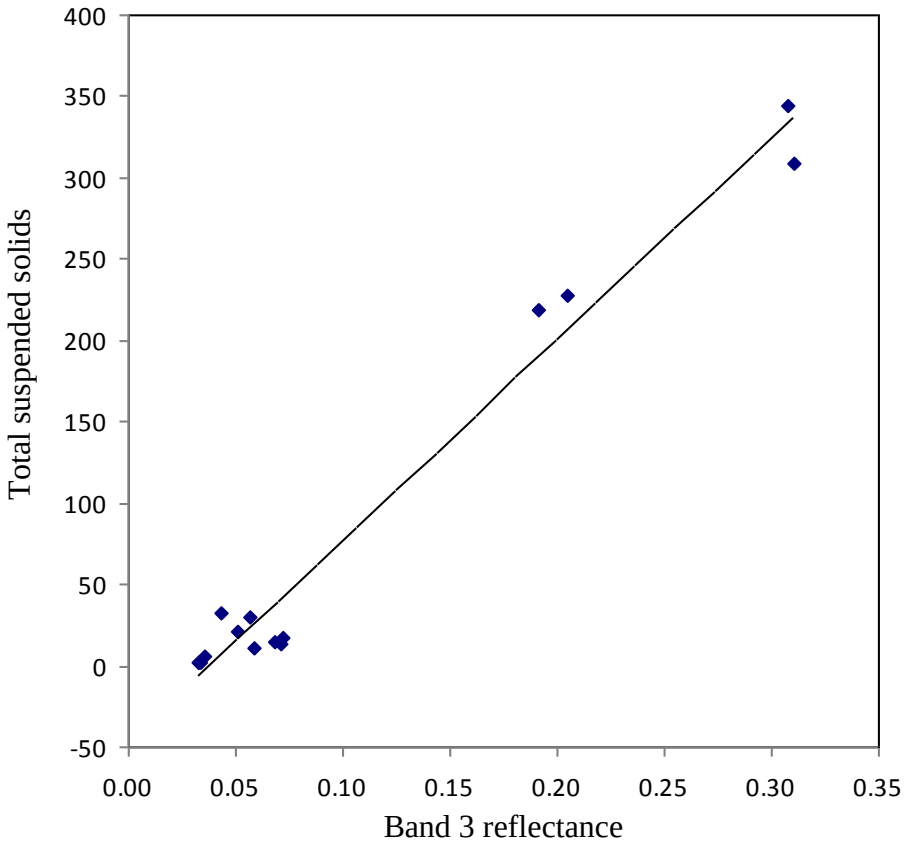


Figure 3.2. TSS vs. Band 3, combined data from 31 March 2000 and 28 August 2002 corresponding to equation 3.4.

High spatial variation was observed in both images, especially in the large riverine lakes Waikare and Whangape (Figures 3.3 and 3.4). On 28 August, Lake Waikare had an *in situ* chl *a* concentration of 150 µg $l^{-1}$ combined with very high TSS concentrations (250 mg $l^{-1}$). Higher TSS concentrations can be seen in the northeast near to the outlet, with relatively clearer water entering from an inlet in the northwest (Figure 3.3). The predicted TSS map for Lake Whangape also shows high spatial variation, with higher TSS concentrations in the main arm of the lake. However on 31 March 2000 higher concentrations of TSS were present in the southern and northwest arms of the lake.

On 31 March 2000 (Figure 3.4), there was less spatial variation of TSS Lake Waikare, combined with relatively low chl *a* concentrations (<20 µg $l^{-1}$). An area of relatively high TSS can be observed were a stream enters the lake in the west.

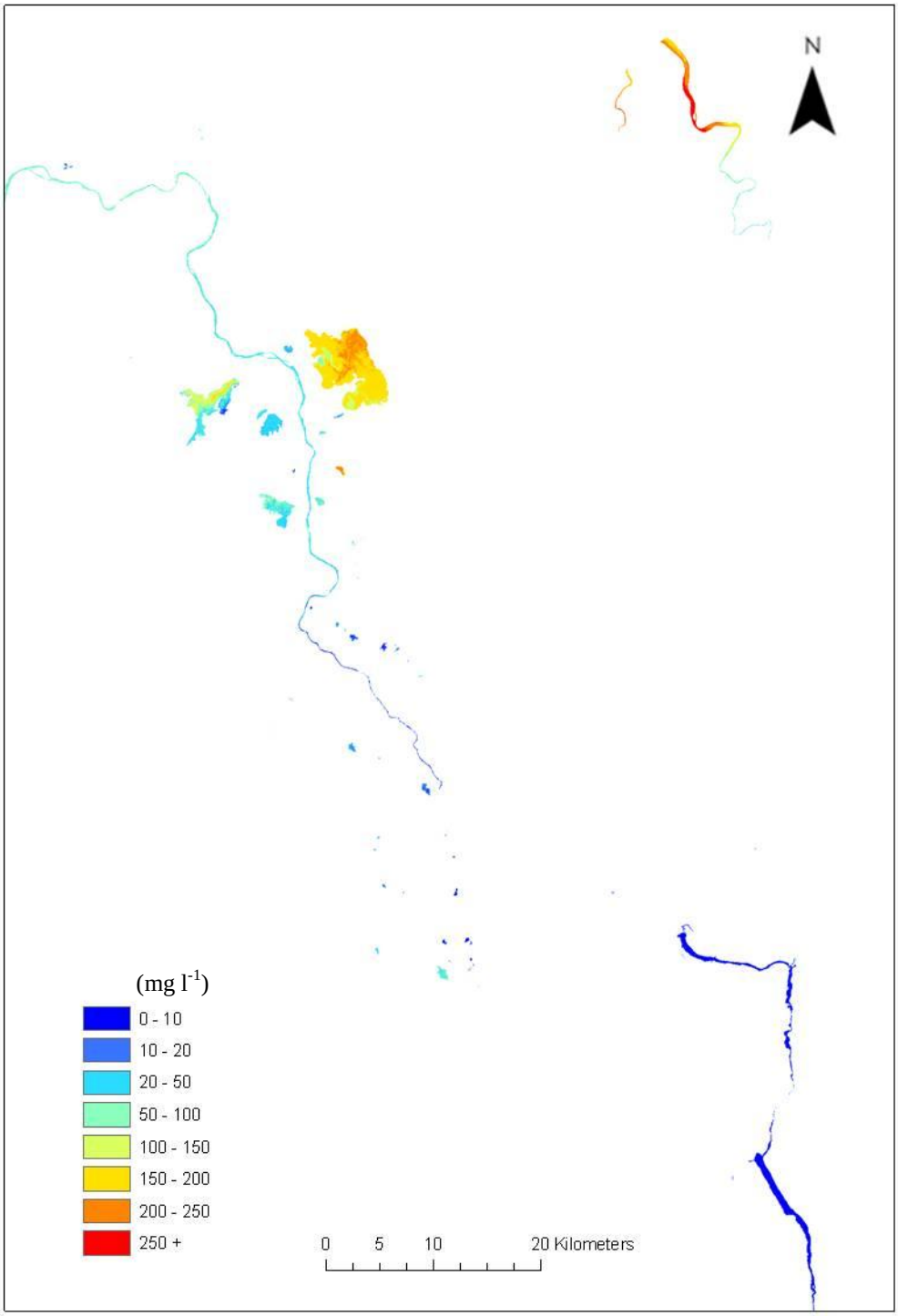


Figure 3.3. TSS on 28 August 2002 predicted from equation 3.4.

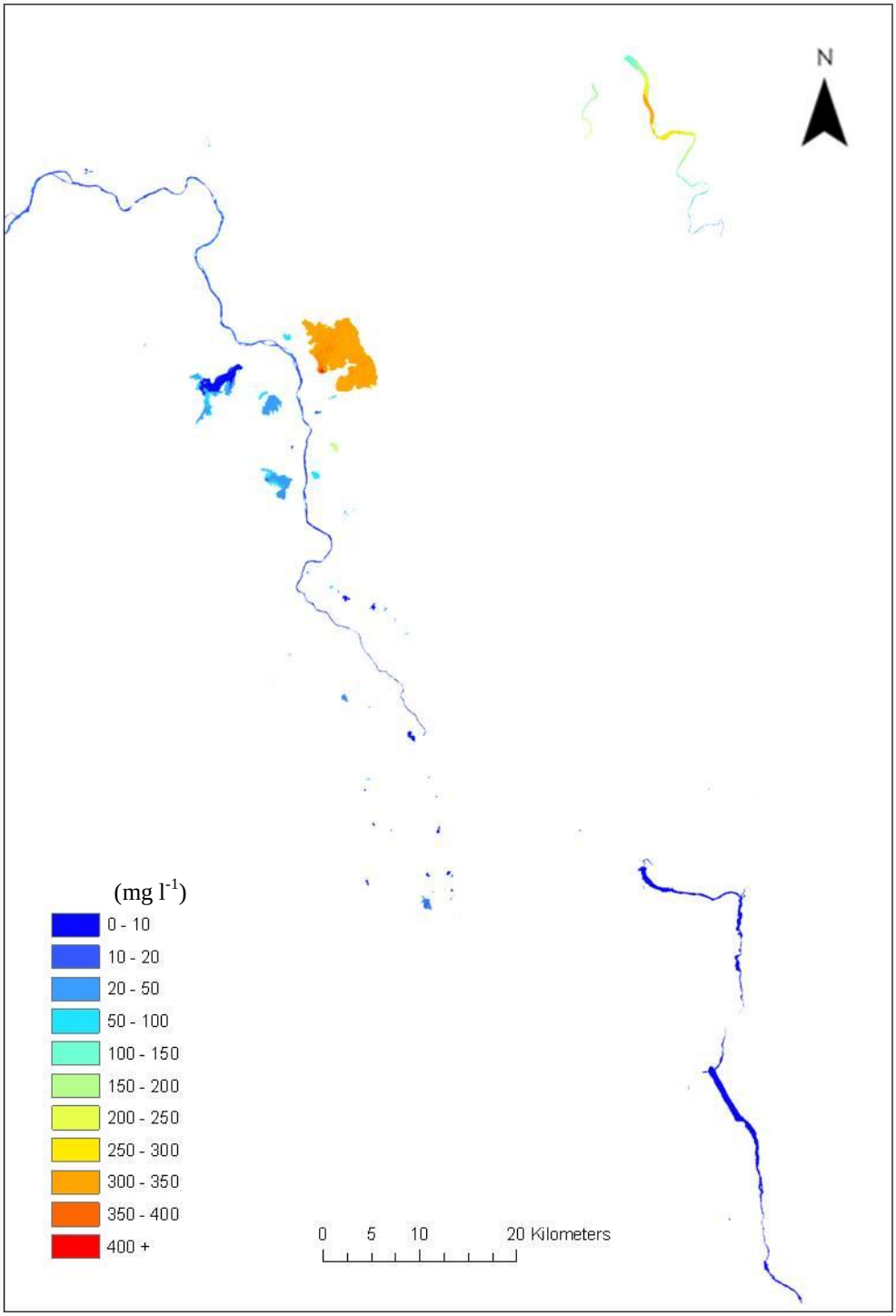


Figure 3.4. TSS concentration on 31 March 2000 predicted from equation 3.4.

### *3.4.3 Linear mixture modelling of raw data*

Landsat bands 1, 2, and 3 were used as input into the mixture model. High correlation already existed between *in situ* samples of chl *a* and *in situ* samples of TSS. The location of endmembers in feature space is shown in Figure 3.5. The final regression equation used to produce the chl *a* concentration map in Figure 3.7 was

Chl *a* = 5.7298 + 2.527 * (Chl endmember percentage) equation 3.5,

where chl *a* is measured in µg $l^{-1}$, $r^2$ = 0.842, *N* = 6, and *p* = 0.001 (see Figure 3.6 for data).

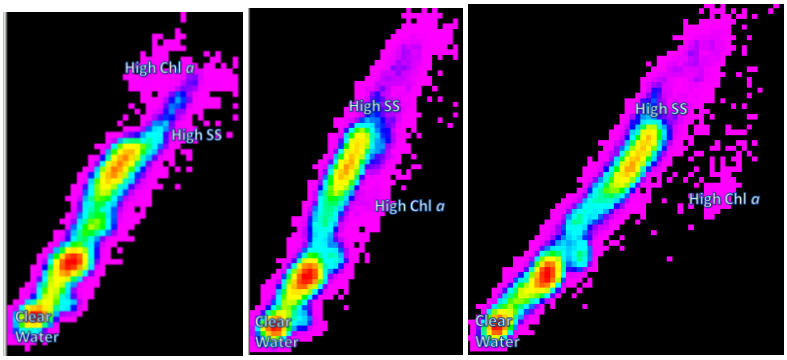


Figure 3.5. Feature space plots and endmember selection using raw data for 24 August 2002, Band 1 vs. Band 2, Band 1 vs. Band 3, and Band 2 vs. Band 3.

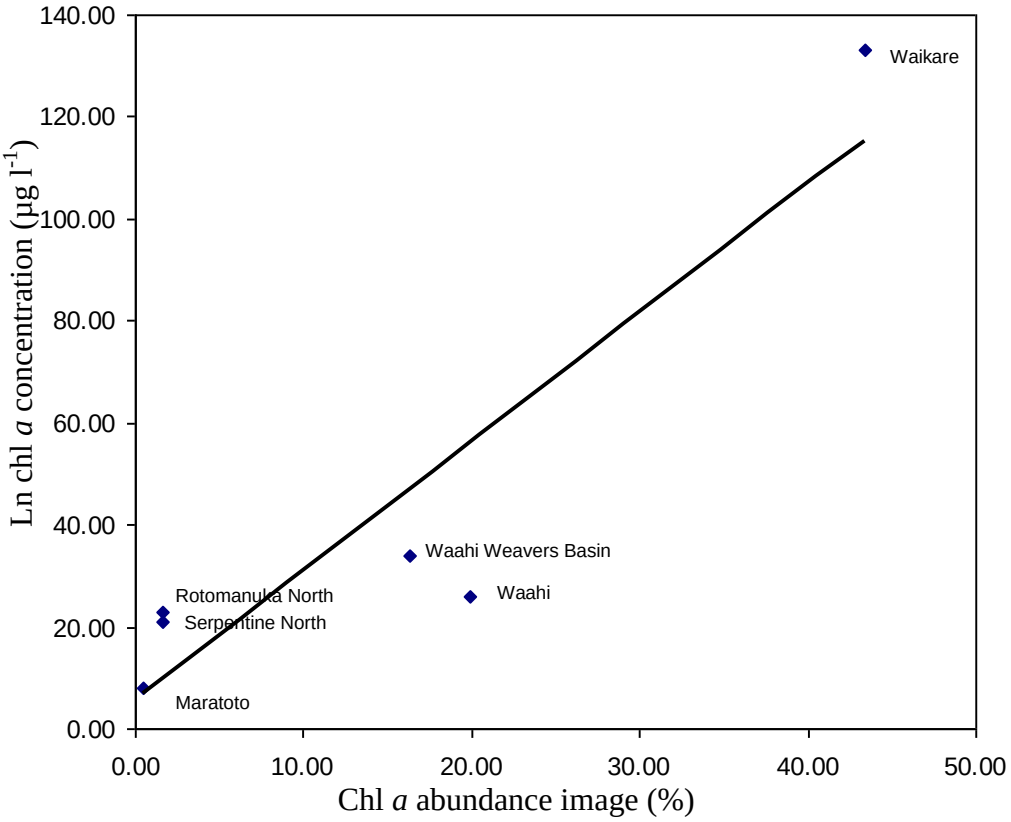


Figure 3.6. Regression of 28 August 2002 chl *a* percentage abundance image and *in situ* chl *a*. for shallow Waikato lakes corresponding to equation 3.5.

This regression produced a chl *a* concentration map that showed different patterns of spatial variation than the TSS concentration maps. This revealed patterns of spatial variation of chl *a* in Lake Waikare where the highest concentrations were found in the southern and north-western areas of the lake.

The correlation between in situ data and water quality parameters is shown in Table 3.2. The high TSS endmember showed a high correlation to all water quality parameters except Secchi depth, which had a higher correlation to the high chl endmember.

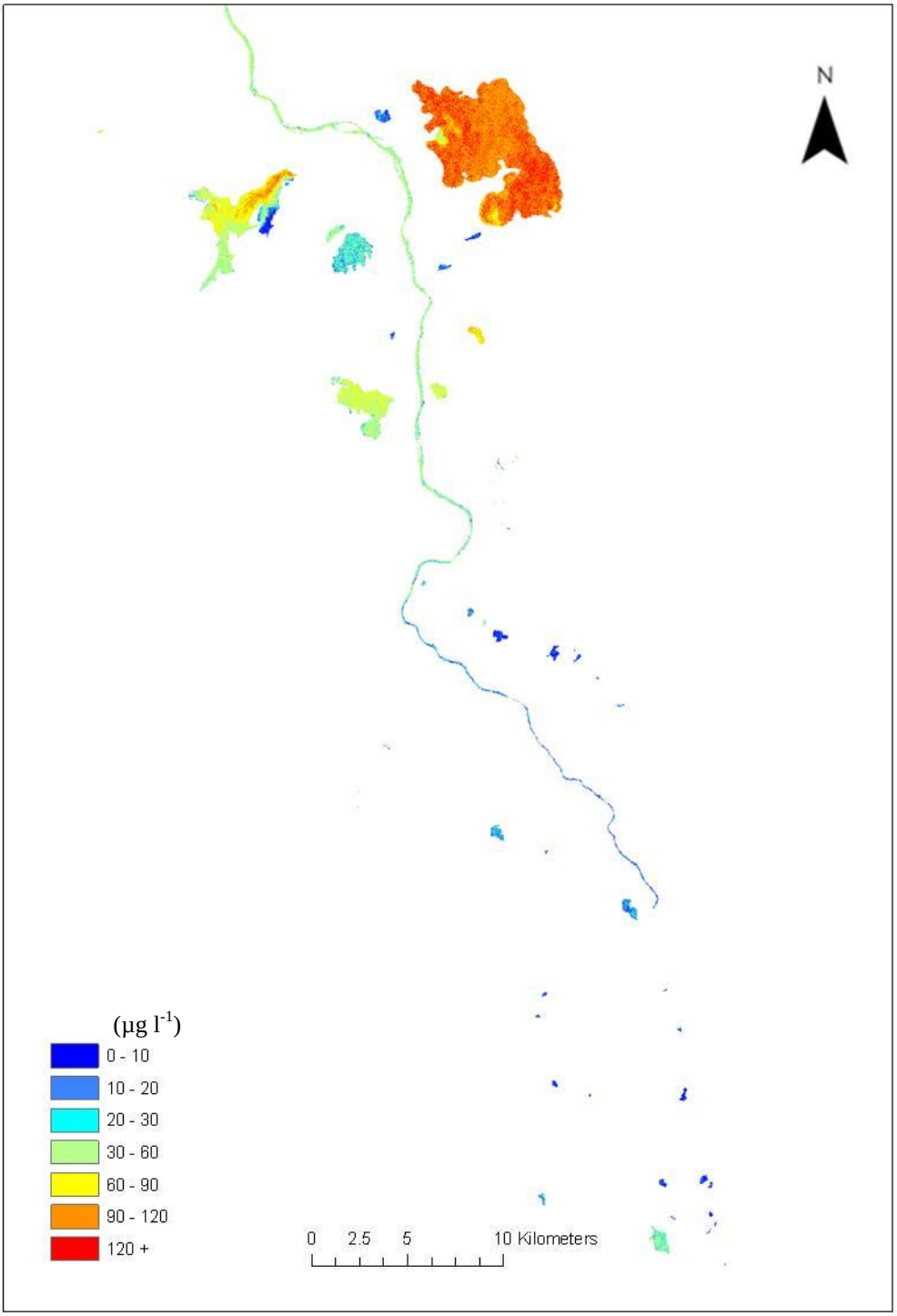


Figure 3.7. Waikato lakes chl *a* concentration (µg $l^{-1}$) on the 28 August 2002 predicted from equation 3.5.

Table 3.2. Most significant correlations of *in situ* data with raw data unmixing endmember fraction images for 28 Aug 2002 (significant correlations in bold, refer to Table 3.1 for abbreviations and units).

| Mixture fraction | Chl *a* | Secchi | TSS | TKN | TP | Turbidity | VSS |
|---|---|---|---|---|---|---|---|
| Clear water | **-0.970** | 0.776 | **-0.975** | -0.798 | **-0.945** | **-0.970** | **-0.962** |
| | **p<0.001** | p=0.068 | **p<0.001** | p=0.057 | **p=0.005** | **p<0.001** | **p=0.002** |
| High chl | **0.916** | **-0.851** | **0.926** | 0.698 | **0.878** | **0.916** | **0.904** |
| | **p=.010** | **p=0.032** | **p=0.003** | p=0.123 | **p=0.021** | **p=0.004** | **p=0.013** |
| High TSS | **0.994** | -0.692 | **0.995** | **0.873** | **0.983** | **0.993** | **0.993** |
| | **p<0.001** | p=0.128 | **p<0.001** | **p=0.023** | **p<0.001** | **p<0.001** | **p<0.001** |

### *3.4.4 Linear Mixture Modelling of PCA transformed data*

TSS fraction maps when calibrated with ground data also produced high correlation with *in situ* samples. However, appropriate endmembers for chl *a* have thus far been difficult to define (Figure 3.8). The resulting chl *a* fraction image does not recognise Lake Waikare as having the highest fraction of the endmember, as Lake Waahi has higher percentage of chl *a* in the fraction image. However, *in situ* chl *a* shows a high correlation to the SS unmixing fraction image (Table 3.2) due to the high covariance of *in situ* chl *a* and TSS.

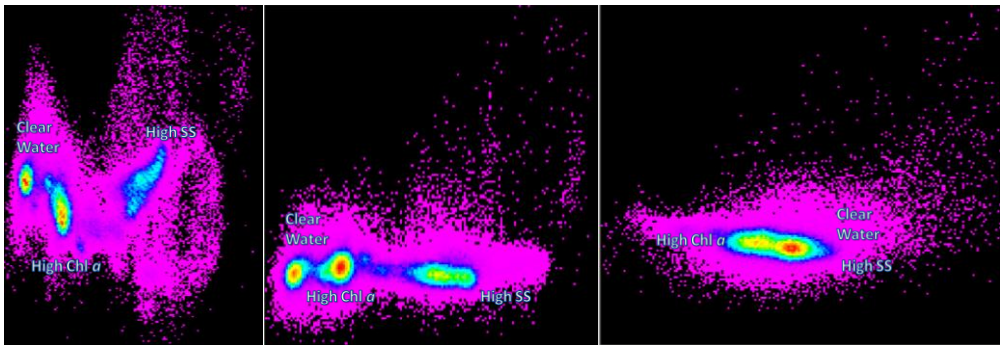


Figure 3.8. Feature space plots and endmember selection using PCA data for 28 August 2002, PC1 vs. PC2, PC1 vs. PC3, PC 2 vs. PC3.

Using the same endmembers as were used to unmix the raw images results in chl *a* fraction images with a value of zero for lakes with low chl *a* concentration (negative abundance estimate). However, the unmixed fraction images also show high spatial variation of chl *a* and TSS in Lake Waikare showing a similar pattern to the raw unmixed chl *a* abundance image.

Table 3.3. Most significant correlations of *in situ* data with PCA unmixing endmember fraction images for 28 August 2002 (significant correlations in bold, refer to Table 3.1 for abbreviations and units).

| Mixture fraction | Chl *a* | Secchi | TSS | TKN | TP | Turbidity | VSS |
|---|---|---|---|---|---|---|---|
| Clear water | -0.752 | **0.912** | -0.716 | -0.436 | -0.681 | -0.699 | -0.724 |
| | p=.084 | **p=0.011** | p=0.110 | p=0.388 | p=0.137 | p=0.122 | p=0.104 |
| High chl | 0.194 | -0.739 | 0.132 | -0.205 | 0.084 | 0.108 | 0.144 |
| | p=0.713 | p=0.094 | p=0.803 | p=0.696 | p=0.875 | p=0.838 | p=0.786 |
| High TSS | **0.986** | -0.611 | **0.999** | **0.941** | **0.999** | **1.000** | **0.998** |
| | **p<0.001** | p=0.198 | **p<0.001** | **p=0.005** | **p<0.001** | **p<0.001** | **p<0.001** |

## 3.5 Discussion

The high correlation achieved between Band 3 and *in situ* reflectance in both images confirms that TSS is readily mapped from Landsat data, and that the results presented here are comparable to other studies (eg. Tyler *et al*., 2006). The range of TSS concentrations covered in this study is larger than in any other previously published work this author could find. The high TSS concentrations in Lake Waikare may be masking the signature of chl *a* to some extent, although patterns of spatial variation of chl *a* were identified in the 28 August 2002 image. The high TSS levels may be responsible for lower chl *a* levels near the outlet due to the lack of light penetration (Barnes, 2002).

On March 31 2000, TSS concentrations in Lake Waikare were higher and less spatial variation of TSS was observed. Chl *a* concentration was < 20 $\mu g\ l^{-1}$, while blooms were observed in surrounding lakes. Again, light limitation caused by high suspended sediment concentrations may have been responsible for low chl *a* at this time.

The final chl *a* regression model has only six *in situ* sample data points and is heavily influenced by Lake Waikare. Also, the high covariance between *in situ* chl *a* and TSS complicates the interpretation of results. However, the resulting chl *a* concentration prediction map shows a pattern of spatial variation different to that of TSS.

Due to the large range in chl *a* and TSS, a non-linear mixture model may be more appropriate where the endmembers selected correspond to different ranges of water quality parameter concentration (Igamberdiev and Lennartz, 2007). In the Waikato lakes this may mean different endmembers are needed for peat lakes and riverine lakes. Riverine lakes in this study had the highest TSS levels combined with relatively high chl *a*, whereas peat lakes had relatively lower levels of TSS, but still high levels of chl *a*.

To investigate a non-linear mixture model, the sample size will have to be larger, and accommodate a wider range of samples from both peat and riverine lakes. I suggest that Lake Whangape should be included in future *in situ* data collection, as the consistent high spatial variation of water quality between the arms and body of the lake would enable a large range of water quality concentration to be sampled in a small time frame and area. Also, sampling of peat lakes needs to be concentrated on larger lakes to lessen the effect of data noise that can be found in the 3 by 3 image

area of interest sample windows that were used (Kloiber, 2002). In March, the negative chl *a* abundance estimates for low chl *a* lakes may also be avoided using a non-linear model, as endmembers will be closer geometrically to data point clusters.

In this study, there was difficulty finding appropriate endmembers due to a number of factors. The ERDAS Imagine software used could identify where a selected pixel on the image lies in feature space plots but not vice versa. This means that the location of endmember pixels (at apexes of the data cloud) was sometimes difficult to determine. In future studies it is recommended that ENVI image analysis should be used, which would enable spatial data reduction using the pixel purity index, and endmember selection using a n-Dimensional Visualizer (Kruse *et al*., 1993).

DOM was not measured and will have to be taken into account in future studies. Its influence on remote sensing reflectance from water is greatest in waters containing high chl *a* and low suspended minerals as is the case in the Waikato peat lakes (Bukata *et al*., 1995). This may contribute to error in retrieval of chl *a* concentrations in these lakes.

Future research should include more *in situ* samples, improved endmember selection techniques using the pixel purity index, and N-dimensional viewer. Furthermore, images should be converted to reflection so endmembers can be applied to images on different dates and endmembers from spectral libraries tested. Also DOM concentrations are yet to be investigated, and may have a significant effect on accuracy of chl *a* retrieval in the Waikato peat lakes.

Using reflectance instead of raw data as an input would mean images from different dates would be radiometrically comparable, and endmembers from spectral

reflectance libraries could be trialed. If adequate atmospheric correction is applied, the same calibration could possibly be applied to other images to predict water quality parameters without *in situ* data.

The application of this approach using platforms with better spectral resolution enabling the diagnostic investigation of the chl *a* signature may produce more accurate results and enable a lower minimum detection limit for chl *a*.

## 3.6 Conclusion

SS was readily mapped using B3, confirming the results of other studies. Chl *a* also showed high correlation to reflectance in the visible and near infrared bands, but high covariance with SS was present. A linear mixture modelling approach was used to map chl *a* concentration ($r^2 = 0.85$).

This approach has been shown to be a cost-effective technique of monitoring spatial variation of water quality, especially in lakes Waikare, Whangape and Waahi. In Whangape and Waikare a different pattern of spatial variation was observed in March 2000 and August 2002. High and heterogeneous concentrations of chl *a* and TSS were observed in both images, with clear patterns of trophic status variation within and between lakes.

# 4. Synthesis

## 4.1 Conclusions

The first objective of this study was to determine empirical models between Landsat imagery and lake water quality variables of the Rotorua lakes. This enabled water quality variables to be synoptically quantified. Analysis was carried out on two Landsat 7 Enhanced Thematic Mapper (ETM+) satellite images of the Rotorua lakes and Lake Taupo, for which most *in situ* observations were taken within 4 days of image capture. Regression equations were developed between the Band 1/Band 3 from Landsat images from summer (25 January 2002) and spring (24 October 2002) and water quality variables measured in the lakes by Environment Bay of Plenty. High correlation was found between ratios and *in situ* data and the maps produced proved useful for analysing spatial distribution of phytoplankton, especially in lakes Rotoiti and Rotoehu.

Application of linear spectral unmixing to the Rotorua lakes may improve the accuracy of chlorophyll (chl) *a* retrieval as the influence of suspended sediments (SS) in shallow lakes may be quantified. For example in shallow lakes such as Lake Rotorua suspended sediment can be a major colour producing agent. Linear spectral unmixing may improve the accuracy of chl *a* retrieval in these lakes by unmixing the signature of chl *a* and SS.

The second objective of this study was to predict total suspended solid (TSS) concentrations in the Waikato lakes using a Band 3 regression model. The high correlation between the atmospherically corrected reflection in Band 3 and *in situ*

TSS concentrations meant this objective was also achieved. This relationship showed temporal stability over the two images, indicating that it may be able to predict TSS with no *in situ* data.

The third objective of this study was to investigate linear mixture modelling to investigate the more optically complex lakes of the Waikato. This technique was successful in unmixing the signatures of clear water, chl *a* and TSS. The resulting maps of chl *a* and TSS showed significant detail on the distribution of phytoplankton and suspended solids. More work is still needed in the area of endmember selection but the results of this study suggest that this method is applicable to the Waikato lakes.

Since remote sensing cannot provide data on all water quality parameters *in situ* monitoring will be necessary in the future. However when *in situ* monitoring combined with remote sensing more lakes can be monitored and monitoring accuracy can be increased in lakes with high spatial variation of water quality. This work has possible applications in lake management. The thematic water quality can be used to pinpoint problem areas. For example areas of elevated turbidity can indicate erosion problems. This method could be applied to previously unmonitored lakes to assess changes in water quality due to landuse changes and introductions of pest fish. These models are applicable to other areas, however models still need to be calibrated with ground data.

# References

Abbott, M. R., Chelton, D. B. (1991). Advances in passive remote sensing of the ocean. *Reviews of. Geophysics* 29: 571-589.

Albet, A. and Mobley, C. D. (2003). An analytical model for subsurface irradiance and remote sensing reflectance in deep and shallow case-2 waters. *Optics Express* 11: 2873-2890.

Baban, S. M. J. (1993a). Detecting water quality parameters in Norfolk Broads. *International Journal of Remote Sensing* 14: 1247-1267.

Baban, S. M. J. (1993b). Detecting and evaluating the influence of water depth, volume and attitude on the variations in the surface temperature of lakes using Landsat Imagery. *International Journal of Remote Sensing* 15: 2747–2758.

Baban, S. M. J. (1999). Use of remote sensing and geographical information systems in developing lake management strategies. *Hydrobiologia* 395/396: 211–226.

Barnes, G. E. (2002). *Water quality trends in Lake Rotomanuka North – implications for restoration and management*. Environment Waikato Technical Report, 2002/03, Hamilton. 19p.

Boswell, J., Russ, Simons, M. (1985). *Waikato small lakes : resource statement*.

Waikato Valley Authority, Hamilton. 130p.

Brown, D., Warwick, R., Skaggs, R. (1977). *Reconnaissance analysis of lake condition in east–central Minnesota*. Report No. 5022. Minnesota land management information system, Center for Urban and Regional Affairs, University of Minnesota, Minneapolis, MN. 19 p.

Burger, D. F., Hamilton, D. P, Hall, J. A., Ryan, E. F. (2007). Phytoplankton nutrient limitation in a polymictic eutrophic lake: community versus species-specific responses. Fundamental and Applied Limnology - *Archiv für Hydrobiologie* 169: 57-68.

Bukata, R. P., Jerome, J. H., Kondratyev, K. Y., Pozdnyakov, D. V. (1995). *Optical properties and remote sensing of inland and coastal waters*. CRC Press, Boka Raton, Florida, USA.

Bricaud, A., Morel, A., Prieur, L. (1981). Absorption by dissolved organic matter of the sea (yellow substance) in the UV and visible domains. *Limnology and Oceanography* 26: 43-53.

Burns, N. M., Rutherford, J. C., Clayton, J. S. (1999). A monitoring and classification system for New Zealand lakes and reservoirs. *Lakes and Reservoir Management* 15: 255-271.

Champion, P. D., de Winton, M. D., de Lange, P. J. (1993). *The vegetation of the lower Waikato lakes*. Volume 2: Vegetation of thirty-eight lakes in the lower Waikato. NIWA Ecosystems Publication No.8. National Institute of Water and Atmospheric Research, Hamilton.

Chavez, P. S. and Jr, (1996). Image-based atmospheric corrections—revisited and revised. *Photogrammetric Engineering and Remote Sensing* 62: 1025-1036.

Curran, P. J. (1985). *Principles of remote sensing*. Longman Group Ltd, London.

Davies-Colley, R. J., Vant, W. N., Smith, D. G. (1993). *Colour and Clarity of Natural Waters*. Ellis Horwood, London.

Dekker, A. G., Malthus, T. J., Wijnen, M. M., Seyhan, E. (1992). The effect of spectral bandwidth and positioning on the spectral signature analysis of inland waters. *Remote Sensing of Environment* 41: 211–225.

Dekker, A. G., Voss, R. J., Peters, S. W. M. (2002). Analytical algorithms for lake water TSM estimation for retrospective analysis of TM and SPOT sensor data. *International Journal of Remote Sensing* 23: 15-35.

Dell, P. (1988). *Lake Waahi catchment water and soil management plan*. Waikato Catchment Board. Technical Publication Number 56.

Gibbons-Davies, J. (2003). *Rotorua Lakes Water Quality 2002*. Environmental Publication 2003/02. Environment Bay of Plenty, Whakatane, New Zealand.

Gibbs, M. (2004). *Lake Taupo Long-Term Monitoring Programme 2002-2003*: Including Two Additional Sites. Environment Waikato Technical Report 2004/05. Environment Waikato, Hamilton East, New Zealand.

Hadjimitsis, D. G., Clayton, C. R. I., Hope, V. S. (2004). An assessment of the effectiveness of atmospheric correction algorithms through remote sensing of some reservoirs. *International Journal of Remote Sensing* 20: 3651–3674.

Hamilton, D. P. (2003). *An historical and contemporary review of water quality in the Rotorua lakes*. Proceedings, Rotorua Lakes 2003, Practical Management for Good Lake Water Quality conference. p 3-15.

Han, L. (1997). Spectral reflectance with varying suspended sediment concentrations in clear and algal-laden waters. *Photogrammetric Engineering and Remote Sensing* 63: 701-705.

Igamberdiev, R., Lennartz, B. (2007). Assessing inland surface water quality by means of hyperspectral remote sensing – A literature review. *Geophysical Research Abstracts* 9: 03376.

Kallio, K., Koponen, S., Pulliainen, J. (2003). Feasibility of airborne imaging spectrometry for lake monitoring-a case study of spatial chlorophyll *a* distribution in two meso-eutrophic lakes. *International Journal of Remote Sensing* 24: 3771-3790.

Kloiber, S. M., Brezonik, P. L., Olmanson, L. G., Bauer, M. E. (2002a). A procedure for regional water clarity assessment using Landsat multispectral data. *Remote Sensing of Environment* 82: 38-47.

Kloiber, S. M., Brezonik, P. L., Bauer, M. E. (2002b). Application of Landsat imagery to regional-scale assessments of lake clarity. *Water Research* 36: 4330-4340.

Kirk, J. T. O. (1988). Optical water quality – what does it mean and how should we measure it? *Journal of the Water Pollution Control Federation* 60: 194-197.

Kirk, J. T. O. (1983) *Light and photosynthesis in aquatic ecosystems*. Cambridge University Press, Cambridge.

Koponen, S. (2006). *Remote sensing of water quality for Finnish lakes and coastal areas*. Doctor of Science dissertation, Helsinki University of Technology, Finland.

Kruse, F. A., Lefkoff, A. B., Boardman, J. W., Heidebrecht, K. B., Shapiro, A. T., Barloon, P. J., A.F.H., G. (1993). The spectral image-processing system (Sips) - interactive visualization and analysis of imaging spectrometer data. *Remote Sensing of Environment* 44: 145-163.

Landsat 7 science data users handbook. Internet website: http://landsathandbook.gsfc.nasa.gov/handbook. Last update: 10.01.2008. Accessed: 27.10.2008.

Lindell, T., Pierson, D., Premazzi, G. and Zilioli, E. (Eds), (1999). *Manual for Monitoring European lakes using remote sensing techniques, part III remote sensing of lakes*. : European Commission Joint Research Centre, Environment Institute, Salmon, Italy. p 81–122.

Lillesand T. M., Johnson W. L., Deuell R. L., Lindstrom O. M., Meisner D. E. (1983). Use of Landsat data to predict the trophic state of Minnesota Lakes. *Photogrammetric Engineering and Remote Sensing* 49: 219-229.

Lowe, D.J., and Green J.D. (1987). *Origins and development of lakes*. In Viner, AB (ed). Inland Waters of New Zealand. DSIR Bulletin 241, Wellington. p 1-64

Mather, P. M. (2005). *Computer Processing of Remotely Sensed Images*. Wiley, West Sussex, England.

Mayo, M., Gitelson**,** A., Ben-Avraham, Z. (1995). Chlorophyll distribution in Lake Kinneret determined from Landsat Thematic Mapper data. *International Journal of Remote Sensing* 16: 175-182.

Morgenstern, U., Gordon, D. (2006). *Prediction of future nitrogen loading to Lake Rotorua*. GNS Science consultancy report 2006/10. pp *2*8.

Nurenburg, G. K., Shaw, M. (1998). Productivity of clear and humic lakes: Nutrients, phytoplankton, bacteria. *Hydobiologica* 382: 97-112.

Oestlund, C., Flink, P., Stroembeck, N., Pierson, D., Lindell, T. (2001). Mapping water quality in Lake Erken, Sweden, from Imaging Spectrometry and Landsat Thematic Mapper. *The Science of the Total Environment* 268: 139-154.

Oliver, R., Ganf, G. (2000). *Freshwater blooms*. In Whitton, B., and Potts, M. (eds), The ecology of Cyanobacteria: their diversity in time and space, The Netherlands: Kluwer Academic Publishers. p 149-194

Olmanson, L. G., Kloiber, S. M., Bauer, M. E., Brezonik, P. L. (2001). *Image processing protocol for regional assessments of lake water quality*. Water Resources Centre and Remote Sensing Laboratory, University of Minnesota.

Preisendorfer, R. W. (1961). Application of radiative transfer theory to light measurements in the sea. *International Union of Geodesy and Geophysics Monographs* 10: 11-29.

Pulliainen, J., Kallio K., Eloheimo, K., Koponen S., Servomaa, H., Hannonen, T., Tauriainen, S., Hallikainen M. (2001). A semi-operative approach to lake water quality retrieval from remote sensing data. *Science of the Total Environment* 268: 79-93.

Ray, D., Gibbs, M., Broekhuizen, N., Rutherford, K., Stephens, S. (2002). *Okawa Bay water quality study*. NIWA Client Report HAM2002-030. National Institute of Water and Atmospheric Research, Hamilton.

Reeves, P., Craggs, R., Stephens, S., de Winton, M., Davies-Colley, R. (2002). *Environmental changes at Lake Waikare, North Waikato*. Wave climate, water quality and biology. NIWA Client Report EVW02235. National Institute of Water and Atmospheric Research, Hamilton.

Rudorff, C. M., Novo, E. M. L. M., Galvão, L. S. (2006). Spectral mixture analysis for water quality assessment over the Amazon floodplain using Hyperion/EO-1 Images. *Revista Ambi_Agua* 1: 65 -79.

Scholes, P., Bloxham, M. (2007). *Rotorua lakes water quality 2006*. Environmental Publication 2007/12. Environment Bay of Plenty, Whakatane, New Zealand.

Small, C. (2004). The Landsat ETM+ spectral mixing space. *Remote Sensing of Environment* 93: 1-17.

Smith, M., O., Johnson, P. E., Adams, J. B. (1985). Quantitative determination of mineral types and abundances from reflectance spectra using principal components analysis. *Journal of Geophysical Research* 90: 792-804.

Stephens, S., de Winton, M.,. Sukias, J., Ovenden, R., Taumoepeau, A., Cooke, J. (2004). Rehabilitation of Lake Waikare: Experimental investigations of the potential benefits of water level drawdown. *Environment Waikato Technical Report,* 2004/25.

Svab, E., Tyler, A. N., Preston, T., Presing, M., Balogh, K. V. (2005). Characterization of the spectral reflectance of algae in lake waters with high suspended sediment concentrations. *International Journal of Remote Sensing* 26: 919–928.

Theimann, S., Kaufmann, H. (2000). Determination of chlorophyll content and trophic state of lakes using field spectrometer and IRS-1C satellite data in the Mecklenburg Lake District, Germany. *Remote Sensing of Environment* 73: 227–235.

Tyler, A. N., Svab, E., Preston, T., Presing, M., Kovacs, W. A. (2006). Remote sensing of the water quality of shallow lakes: A mixture modelling approach to quantifying phytoplankton in water characterized by high-suspended sediment. *International Journal of Remote Sensing* 27: 1521-1537.

Vant, W. N. (1987). Lake Whangape – muddy waters and macrophytes. *Soil & Water* 23: 20-24.

Vant, W. N., Davies-Colley, R. J. (1986). Relative importance of clarity determinants in lakes Okaro and Rotorua. *New Zealand Journal of Marine and Freshwater Research* 20: 355-363.

Van Der Meer, F., De Jong, S. M. (2000). Improving the results of spectral unmixing of Landsat Thematic Mapper imagery by enhancing the orthogonality of end-members. *International Journal of Remote Sensing* 21: 2781-297.

Wells, R.D.S., Vant, W. N., Clayton, J. S. (1988). Inorganic suspensoids and submerged macrophytes in Lake Whangape, New Zealand. *Verh. Internat. Verein. Limnol.* 23: 1969-1972.

Wetzel, R. G. (2001). Limnology*: Lake and River Ecosystems*. 3rd Edition. Academic Press.

White, E., Law, K., Payne, S., Pickmore, S. (1985). Nutrient demand and availability among planktonic communities – an attempt to assess nutrient limitation to plant growth in 12 Central Volcanic Plateau lakes. *New Zealand Journal of Marine and Freshwater Research* 19: 49-62.

Yentch, C. S., Yentsch, C. M. (1979). Flourescence spectral signatures: the characterization of phytoplankton populations by the use of exitation and emission spectra. *Journal of Marine Research* 37: 471-483.

Zhang, Y., Pulliainen, J., Koponen, S., Hallikainen, M. (2002). Application of an empirical neural network to surface water quality estimation in the Gulf of Finland using combined optical data and microwave data. *Remote Sensing of Environment* 81: 327-336.

Zilioli, E., Brivio, P. A. (1996). The satellite derived optical information for the comparative assessment of lacustrine water quality. *Science of the Total Environment* 196: 229-245.

# Appendices

**Appendix1. EBOP unpublished water quality data and satellite data from Landsat 7 ETM+ image.**

*1A. 25 January 2002 image and data.*

| Site | Date | Chl *a* (µg/L) | Secchi depth (m) | Turbidity (NTU) | B1 | B2 | B3 | B1/B3 | (B1-B3)/B2 |
|---|---|---|---|---|---|---|---|---|---|
| Taupo site C | 22-Jan-02 | 0.8 | 15.5 | | 61.6 | 34.3 | 22.5 | 2.74 | 1.14 |
| Taupo site A | 22-Jan-02 | 0.9 | 15.0 | | 61.9 | 34.7 | 22.1 | 2.80 | 1.15 |
| Okareka site 1 | 23-Jan-02 | 1.4 | 10.2 | 0.57 | 57.9 | 33.9 | 22.1 | 2.62 | 1.06 |
| Tarawera site 5 | 23-Jan-02 | 2.1 | 9.4 | 0.42 | 62.1 | 35.8 | 22.9 | 2.72 | 1.10 |
| Rerewhakaaitu site 1 | 9-Jan-02 | 2.4 | 5.5 | 0.70 | 57.8 | 35.0 | 22.5 | 2.57 | 1.01 |
| Okataina site 1 | 22-Jan-02 | 3.1 | 9.8 | 0.54 | 59.5 | 35.2 | 23.6 | 2.52 | 1.02 |
| Rotokakahi site 10 | 23-Jan-02 | 3.3 | | 0.69 | 59.3 | 35.2 | 23.4 | 2.53 | 1.02 |
| Tikitapu site 1 | 23-Jan-02 | 4.4 | 4.2 | 0.85 | 62.2 | 39.9 | 23.8 | 2.62 | 0.96 |
| Rotoiti site 4 | 22-Jan-02 | 6.0 | 4.3 | 0.95 | 61.2 | 37.3 | 23.6 | 2.59 | 1.01 |
| Rotoiti Te Weta site | 17-Jan-02 | 10.4 | | 2.60 | 60.6 | 39.6 | 26.4 | 2.30 | 0.86 |
| Rotoiti site 3 | 22-Jan-02 | 11.5 | 3.5 | 1.90 | 62.2 | 42.1 | 26.9 | 2.32 | 0.84 |
| Rotorua site 2 | 23-Jan-02 | 16.5 | 4.5 | 2.20 | 59.6 | 38.2 | 26.3 | 2.27 | 0.87 |
| Rotorua site 5 | 23-Jan-02 | 17.6 | 2.3 | 2.60 | 60.3 | 38.3 | 26.1 | 2.31 | 0.89 |
| Rotoiti western basin site | 24-Jan-02 | 19.4 | 2.7 | 3.30 | 62.6 | 42.9 | 27.7 | 2.26 | 0.81 |
| Rotoehu site 3 | 22-Jan-02 | 25.0 | 2.0 | 2.60 | 62.8 | 49.0 | 31.3 | 2.01 | 0.64 |
| Rotoiti Okawa Bay site | 24-Jan-02 | 136.0 | 0.8 | 15.00 | 65.3 | 57.1 | 34.6 | 1.89 | 0.54 |

*1B. 24 October 2002 image and data.*

| Site | Date | Chl *a* (µg/L) | Secchi depth (m) | Turbidity (NTU) | B1 | B2 | B3 | B1/B3 | (B1-B3)/B2 |
|---|---|---|---|---|---|---|---|---|---|
| Okareka site 1 | 24/10/2002 | 2.5 | 8.1 | 1.00 | 55.6 | 32.9 | 22.3 | 1.01 | 2.50 |
| Okataina site 1 | 23/10/2002 | 2.9 | 7.5 | 0.67 | 56.0 | 31.8 | 21.8 | 1.08 | 2.57 |
| Rotokakahi site 10 | 24/10/2002 | 2.4 | | 0.68 | 57.1 | 34.5 | 22.5 | 1.00 | 2.53 |
| Rotorua site 2 | 24/10/2002 | 23.8 | 1.9 | 3.50 | 58.4 | 38.1 | 25.8 | 0.86 | 2.27 |
| Rotorua site 5 | 24/10/2002 | 23.6 | 1.9 | 4.60 | 58.1 | 38.3 | 26.3 | 0.83 | 2.21 |
| Tikitapu site 1 | 24/10/2002 | 2.0 | 4.0 | 0.82 | 60.5 | 38.5 | 23.1 | 0.97 | 2.62 |
| Okaro site 1 | 22/10/2002 | 89.1 | 1.3 | 4.50 | 56.5 | 39.4 | 24.9 | 0.80 | 2.27 |
| Rerewhakaaitu site 1 | 22/10/2002 | 1.2 | 10.2 | | 56.4 | 33.9 | 22.5 | 1.00 | 2.51 |
| Rotomahana site 1 | 22/10/2002 | 5.9 | 2.9 | 1.30 | 57.1 | 35.4 | 23.6 | 0.95 | 2.42 |
| Tarawera site 5 | 24/10/2002 | 0.5 | 8.4 | 1.40 | 59.8 | 34.4 | 22.3 | 1.09 | 2.68 |
| Taupo site A | 9/10/2002 | 0.6 | 15.5 | | 58.2 | 32.2 | 21.4 | 1.14 | 2.71 |
| Taupo site B | 9/10/2002 | 0.5 | 15.0 | | 58.3 | 33.1 | 22.9 | 1.07 | 2.54 |
| Taupo site C | 9/10/2002 | 0.4 | 19.0 | | 58.6 | 32.4 | 21.8 | 1.13 | 2.69 |

## Appendix 2- Atmospheric correction parameters

*2A. Landsat ETM+ Solar Spectral Irradiances. Source: Landsat (2002).*

| Landsat band | watts/(meter squared * μm) |
|---|---|
| 1 | 1969.0 |
| 2 | 1840.0 |
| 3 | 1551.0 |
| 4 | 1044.0 |
| 5 | 225.7 |
| 7 | 82.07 |
| 8 | 1368.0 |

*2B. Earth Sun distance in astronomical units (AU). Source: Landsat (2002).*

| Julian Day | Distance | Julian Day | Distance | Julian Day | Distance | Julian Day | Distance | Julian Day | Distance |
|---|---|---|---|---|---|---|---|---|---|
| 1 | 0.9832 | 74 | 0.9945 | 152 | 1.014 | 227 | 1.0128 | 305 | 0.9925 |
| 15 | 0.9836 | 91 | 0.9993 | 166 | 1.0158 | 242 | 1.0092 | 319 | 0.9892 |
| 32 | 0.9853 | 106 | 1.0033 | 182 | 1.0167 | 258 | 1.0057 | 335 | 0.986 |
| 46 | 0.9878 | 121 | 1.0076 | 196 | 1.0165 | 274 | 1.0011 | 349 | 0.9843 |
| 60 | 0.9909 | 135 | 1.0109 | 213 | 1.0149 | 288 | 0.9972 | 365 | 0.9833 |

# Appendix 3- Image metadata

## *3A. Metadata for 31 March 2000*

```
GROUP = METADATA_FILE
        PRODUCT_CREATION_TIME = 2004-02-12T18:15:23Z
        PRODUCT_FILE_SIZE = 665.9
        STATION_ID = "EDC"
        GROUND_STATION = "EDC"
        GROUP = ORTHO_PRODUCT_METADATA
                SPACECRAFT_ID = "Landsat7"
                SENSOR_ID = "ETM+"
                ACQUISITION_DATE = 2000-03-30
                WRS_PATH = 073
                WRS_ROW = 086
                SCENE_CENTER_LAT = -37.4702354
                SCENE_CENTER_LON = +175.2517648
                SCENE_UL_CORNER_LAT = -36.5140039
                SCENE_UL_CORNER_LON = +174.4650560
                SCENE_UR_CORNER_LAT = -36.8118067
                SCENE_UR_CORNER_LON = +176.5194807
                SCENE_LL_CORNER_LAT = -38.1139424
                SCENE_LL_CORNER_LON = +173.9625137
                SCENE_LR_CORNER_LAT = -38.4217119
                SCENE_LR_CORNER_LON = +176.0581327
                SCENE_UL_CORNER_MAPX = 273001.500
                SCENE_UL_CORNER_MAPY = -4043950.500
                SCENE_UR_CORNER_MAPX = 457140.000
                SCENE_UR_CORNER_MAPY = -4074103.500
                SCENE_LL_CORNER_MAPX = 233700.000
                SCENE_LL_CORNER_MAPY = -4222816.500
                SCENE_LR_CORNER_MAPX = 417781.500
                SCENE_LR_CORNER_MAPY = -4253026.500
                BAND1_FILE_NAME = "p073r086_7t20000330_z60_nn10.tif"
                BAND2_FILE_NAME = "p073r086_7t20000330_z60_nn20.tif"
                BAND3_FILE_NAME = "p073r086_7t20000330_z60_nn30.tif"
                BAND4_FILE_NAME = "p073r086_7t20000330_z60_nn40.tif"
                BAND5_FILE_NAME = "p073r086_7t20000330_z60_nn50.tif"
                BAND61_FILE_NAME = "p073r086_7k20000330_z60_nn61.tif"
                BAND62_FILE_NAME = "p073r086_7k20000330_z60_nn62.tif"
                BAND7_FILE_NAME = "p073r086_7t20000330_z60_nn70.tif"
                BAND8_FILE_NAME = "p073r086_7p20000330_z60_nn80.tif"
                GROUP = PROJECTION_PARAMETERS
                        REFERENCE_DATUM = "WGS84"
                        REFERENCE_ELLIPSOID = "WGS84"
                        GRID_CELL_ORIGIN = "Center"
                        UL_GRID_LINE_NUMBER = 1
                        UL_GRID_SAMPLE_NUMBER = 1
                        GRID_INCREMENT_UNIT = "Meters"
                        GRID_CELL_SIZE_PAN = 14.250
                        GRID_CELL_SIZE_THM = 57.000
                        GRID_CELL_SIZE_REF = 28.500
                        FALSE_NORTHING = 0
                        ORIENTATION = "NUP"
                        RESAMPLING_OPTION = "NN"
                        MAP_PROJECTION = "UTM"
                END_GROUP = PROJECTION_PARAMETERS
                GROUP = UTM_PARAMETERS
                        ZONE_NUMBER = +60
```

```
        END_GROUP = UTM_PARAMETERS
        SUN_AZIMUTH = 47.0881386
        SUN_ELEVATION = 36.4946285
        QA_PERCENT_MISSING_DATA = 66
        CLOUD_COVER = 0
        PRODUCT_SAMPLES_PAN = 17360
        PRODUCT_LINES_PAN = 15310
        PRODUCT_SAMPLES_REF = 8680
        PRODUCT_LINES_REF = 7655
        PRODUCT_SAMPLES_THM = 4340
        PRODUCT_LINES_THM = 3828
        OUTPUT_FORMAT = "GEOTIFF"
END_GROUP = ORTHO_PRODUCT_METADATA
GROUP = L1G_PRODUCT_METADATA
        BAND_COMBINATION = "123456678"
        CPF_FILE_NAME = "L7CPF20000101_20000331_12"
        GROUP = MIN_MAX_RADIANCE
                LMAX_BAND1 = 191.600
                LMIN_BAND1 = -6.200
                LMAX_BAND2 = 196.500
                LMIN_BAND2 = -6.400
                LMAX_BAND3 = 152.900
                LMIN_BAND3 = -5.000
                LMAX_BAND4 = 157.400
                LMIN_BAND4 = -5.100
                LMAX_BAND5 = 31.060
                LMIN_BAND5 = -1.000
                LMAX_BAND61 = 17.040
                LMIN_BAND61 = 0.000
                LMAX_BAND62 = 12.650
                LMIN_BAND62 = 3.200
                LMAX_BAND7 = 10.800
                LMIN_BAND7 = -0.350
                LMAX_BAND8 = 243.100
                LMIN_BAND8 = -4.700
        END_GROUP = MIN_MAX_RADIANCE
        GROUP = MIN_MAX_PIXEL_VALUE
                QCALMAX_BAND1 = 255.0
                QCALMIN_BAND1 = 1.0
                QCALMAX_BAND2 = 255.0
                QCALMIN_BAND2 = 1.0
                QCALMAX_BAND3 = 255.0
                QCALMIN_BAND3 = 1.0
                QCALMAX_BAND4 = 255.0
                QCALMIN_BAND4 = 1.0
                QCALMAX_BAND5 = 255.0
                QCALMIN_BAND5 = 1.0
                QCALMAX_BAND61 = 255.0
                QCALMIN_BAND61 = 1.0
                QCALMAX_BAND62 = 255.0
                QCALMIN_BAND62 = 1.0
                QCALMAX_BAND7 = 255.0
                QCALMIN_BAND7 = 1.0
                QCALMAX_BAND8 = 255.0
                QCALMIN_BAND8 = 1.0
        END_GROUP = MIN_MAX_PIXEL_VALUE
        GROUP = PRODUCT_PARAMETERS
                CORRECTION_METHOD_GAIN_BAND1 = "CPF"
                CORRECTION_METHOD_GAIN_BAND2 = "CPF"
                CORRECTION_METHOD_GAIN_BAND3 = "CPF"
                CORRECTION_METHOD_GAIN_BAND4 = "CPF"
                CORRECTION_METHOD_GAIN_BAND5 = "CPF"
```

```
                CORRECTION_METHOD_GAIN_BAND61 = "CPF"
                CORRECTION_METHOD_GAIN_BAND62 = "CPF"
                CORRECTION_METHOD_GAIN_BAND7 = "CPF"
                CORRECTION_METHOD_GAIN_BAND8 = "CPF"
                CORRECTION_METHOD_BIAS = "IC"
                BAND1_GAIN = "H"
                BAND2_GAIN = "H"
                BAND3_GAIN = "H"
                BAND4_GAIN = "H"
                BAND5_GAIN = "H"
                BAND6_GAIN1 = "L"
                BAND6_GAIN2 = "H"
                BAND7_GAIN = "H"
                BAND8_GAIN = "L"
                BAND1_GAIN_CHANGE = "0"
                BAND2_GAIN_CHANGE = "0"
                BAND3_GAIN_CHANGE = "0"
                BAND4_GAIN_CHANGE = "0"
                BAND5_GAIN_CHANGE = "0"
                BAND6_GAIN_CHANGE1 = "0"
                BAND6_GAIN_CHANGE2 = "0"
                BAND7_GAIN_CHANGE = "0"
                BAND8_GAIN_CHANGE = "0"
                BAND1_SL_GAIN_CHANGE = "0"
                BAND2_SL_GAIN_CHANGE = "0"
                BAND3_SL_GAIN_CHANGE = "0"
                BAND4_SL_GAIN_CHANGE = "0"
                BAND5_SL_GAIN_CHANGE = "0"
                BAND6_SL_GAIN_CHANGE1 = "0"
                BAND6_SL_GAIN_CHANGE2 = "0"
                BAND7_SL_GAIN_CHANGE = "0"
                BAND8_SL_GAIN_CHANGE = "0"
        END_GROUP = PRODUCT_PARAMETERS
        GROUP = CORRECTIONS_APPLIED
                STRIPING_BAND1 = "NONE"
                STRIPING_BAND2 = "NONE"
                STRIPING_BAND3 = "NONE"
                STRIPING_BAND4 = "NONE"
                STRIPING_BAND5 = "NONE"
                STRIPING_BAND61 = "NONE"
                STRIPING_BAND62 = "NONE"
                STRIPING_BAND7 = "NONE"
                STRIPING_BAND8 = "NONE"
                BANDING = "N"
                COHERENT_NOISE = "N"
                MEMORY_EFFECT = "N"
                SCAN_CORRELATED_SHIFT = "N"
                INOPERABLE_DETECTORS = "N"
                DROPPED_LINES = Y
        END_GROUP = CORRECTIONS_APPLIED
    END_GROUP = L1G_PRODUCT_METADATA
END_GROUP = METADATA_FILE
END
```

## *3B. Metadata for 28 August 2002*

```
GROUP = METADATA_FILE
    PRODUCT_CREATION_TIME = 2004-02-12T18:15:34Z
    PRODUCT_FILE_SIZE = 676.0
    STATION_ID = "EDC"
```

```
GROUND_STATION = "EDC"
GROUP = ORTHO_PRODUCT_METADATA
        SPACECRAFT_ID = "Landsat7"
        SENSOR_ID = "ETM+"
        ACQUISITION_DATE = 2002-08-27
        WRS_PATH = 073
        WRS_ROW = 086
        SCENE_CENTER_LAT = -37.4731075
        SCENE_CENTER_LON = +175.2592714
        SCENE_UL_CORNER_LAT = -36.5134161
        SCENE_UL_CORNER_LON = +174.4736667
        SCENE_UR_CORNER_LAT = -36.8110680
        SCENE_UR_CORNER_LON = +176.5274733
        SCENE_LL_CORNER_LAT = -38.1205396
        SCENE_LL_CORNER_LON = +173.9693910
        SCENE_LR_CORNER_LAT = -38.4279278
        SCENE_LR_CORNER_LON = +176.0645821
        SCENE_UL_CORNER_MAPX = 273771.000
        SCENE_UL_CORNER_MAPY = -4043865.000
        SCENE_UR_CORNER_MAPX = 457852.500
        SCENE_UR_CORNER_MAPY = -4074018.000
        SCENE_LL_CORNER_MAPX = 234327.000
        SCENE_LL_CORNER_MAPY = -4223529.000
        SCENE_LR_CORNER_MAPX = 418351.500
        SCENE_LR_CORNER_MAPY = -4253710.500
        BAND1_FILE_NAME = "p073r086_7t20020827_z60_nn10.tif"
        BAND2_FILE_NAME = "p073r086_7t20020827_z60_nn20.tif"
        BAND3_FILE_NAME = "p073r086_7t20020827_z60_nn30.tif"
        BAND4_FILE_NAME = "p073r086_7t20020827_z60_nn40.tif"
        BAND5_FILE_NAME = "p073r086_7t20020827_z60_nn50.tif"
        BAND61_FILE_NAME = "p073r086_7k20020827_z60_nn61.tif"
        BAND62_FILE_NAME = "p073r086_7k20020827_z60_nn62.tif"
        BAND7_FILE_NAME = "p073r086_7t20020827_z60_nn70.tif"
        BAND8_FILE_NAME = "p073r086_7p20020827_z60_nn80.tif"
        GROUP = PROJECTION_PARAMETERS
                REFERENCE_DATUM = "WGS84"
                REFERENCE_ELLIPSOID = "WGS84"
                GRID_CELL_ORIGIN = "Center"
                UL_GRID_LINE_NUMBER = 1
                UL_GRID_SAMPLE_NUMBER = 1
                GRID_INCREMENT_UNIT = "Meters"
                GRID_CELL_SIZE_PAN = 14.250
                GRID_CELL_SIZE_THM = 57.000
                GRID_CELL_SIZE_REF = 28.500
                FALSE_NORTHING = 0
                ORIENTATION = "NUP"
                RESAMPLING_OPTION = "NN"
                MAP_PROJECTION = "UTM"
        END_GROUP = PROJECTION_PARAMETERS
        GROUP = UTM_PARAMETERS
                ZONE_NUMBER = +60
        END_GROUP = UTM_PARAMETERS
        SUN_AZIMUTH = 43.5917631
        SUN_ELEVATION = 31.5468078
        QA_PERCENT_MISSING_DATA = 0
        CLOUD_COVER = 0
        PRODUCT_SAMPLES_PAN = 17490
        PRODUCT_LINES_PAN = 15426
        PRODUCT_SAMPLES_REF = 8745
        PRODUCT_LINES_REF = 7713
        PRODUCT_SAMPLES_THM = 4373
        PRODUCT_LINES_THM = 3857
```

```
        OUTPUT_FORMAT = "GEOTIFF"
END_GROUP = ORTHO_PRODUCT_METADATA
GROUP = L1G_PRODUCT_METADATA
        BAND_COMBINATION = "123456678"
        CPF_FILE_NAME = "L7CPF20020701_20020930_04"
        GROUP = MIN_MAX_RADIANCE
                LMAX_BAND1 = 191.600
                LMIN_BAND1 = -6.200
                LMAX_BAND2 = 196.500
                LMIN_BAND2 = -6.400
                LMAX_BAND3 = 152.900
                LMIN_BAND3 = -5.000
                LMAX_BAND4 = 157.400
                LMIN_BAND4 = -5.100
                LMAX_BAND5 = 31.060
                LMIN_BAND5 = -1.000
                LMAX_BAND61 = 17.040
                LMIN_BAND61 = 0.000
                LMAX_BAND62 = 12.650
                LMIN_BAND62 = 3.200
                LMAX_BAND7 = 10.800
                LMIN_BAND7 = -0.350
                LMAX_BAND8 = 243.100
                LMIN_BAND8 = -4.700
        END_GROUP = MIN_MAX_RADIANCE
        GROUP = MIN_MAX_PIXEL_VALUE
                QCALMAX_BAND1 = 255.0
                QCALMIN_BAND1 = 1.0
                QCALMAX_BAND2 = 255.0
                QCALMIN_BAND2 = 1.0
                QCALMAX_BAND3 = 255.0
                QCALMIN_BAND3 = 1.0
                QCALMAX_BAND4 = 255.0
                QCALMIN_BAND4 = 1.0
                QCALMAX_BAND5 = 255.0
                QCALMIN_BAND5 = 1.0
                QCALMAX_BAND61 = 255.0
                QCALMIN_BAND61 = 1.0
                QCALMAX_BAND62 = 255.0
                QCALMIN_BAND62 = 1.0
                QCALMAX_BAND7 = 255.0
                QCALMIN_BAND7 = 1.0
                QCALMAX_BAND8 = 255.0
                QCALMIN_BAND8 = 1.0
        END_GROUP = MIN_MAX_PIXEL_VALUE
        GROUP = PRODUCT_PARAMETERS
                CORRECTION_METHOD_GAIN_BAND1 = "CPF"
                CORRECTION_METHOD_GAIN_BAND2 = "CPF"
                CORRECTION_METHOD_GAIN_BAND3 = "CPF"
                CORRECTION_METHOD_GAIN_BAND4 = "CPF"
                CORRECTION_METHOD_GAIN_BAND5 = "CPF"
                CORRECTION_METHOD_GAIN_BAND61 = "CPF"
                CORRECTION_METHOD_GAIN_BAND62 = "CPF"
                CORRECTION_METHOD_GAIN_BAND7 = "CPF"
                CORRECTION_METHOD_GAIN_BAND8 = "CPF"
                CORRECTION_METHOD_BIAS = "IC"
                BAND1_GAIN = "H"
                BAND2_GAIN = "H"
                BAND3_GAIN = "H"
                BAND4_GAIN = "H"
                BAND5_GAIN = "H"
                BAND6_GAIN1 = "L"
```

```
                BAND6_GAIN2 = "H"
                BAND7_GAIN = "H"
                BAND8_GAIN = "L"
                BAND1_GAIN_CHANGE = "0"
                BAND2_GAIN_CHANGE = "0"
                BAND3_GAIN_CHANGE = "0"
                BAND4_GAIN_CHANGE = "0"
                BAND5_GAIN_CHANGE = "0"
                BAND6_GAIN_CHANGE1 = "0"
                BAND6_GAIN_CHANGE2 = "0"
                BAND7_GAIN_CHANGE = "0"
                BAND8_GAIN_CHANGE = "0"
                BAND1_SL_GAIN_CHANGE = "0"
                BAND2_SL_GAIN_CHANGE = "0"
                BAND3_SL_GAIN_CHANGE = "0"
                BAND4_SL_GAIN_CHANGE = "0"
                BAND5_SL_GAIN_CHANGE = "0"
                BAND6_SL_GAIN_CHANGE1 = "0"
                BAND6_SL_GAIN_CHANGE2 = "0"
                BAND7_SL_GAIN_CHANGE = "0"
                BAND8_SL_GAIN_CHANGE = "0"
        END_GROUP = PRODUCT_PARAMETERS
        GROUP = CORRECTIONS_APPLIED
                STRIPING_BAND1 = "NONE"
                STRIPING_BAND2 = "NONE"
                STRIPING_BAND3 = "NONE"
                STRIPING_BAND4 = "NONE"
                STRIPING_BAND5 = "NONE"
                STRIPING_BAND61 = "NONE"
                STRIPING_BAND62 = "NONE"
                STRIPING_BAND7 = "NONE"
                STRIPING_BAND8 = "NONE"
                BANDING = "N"
                COHERENT_NOISE = "N"
                MEMORY_EFFECT = "N"
                SCAN_CORRELATED_SHIFT = "N"
                INOPERABLE_DETECTORS = "N"
                DROPPED_LINES = N
        END_GROUP = CORRECTIONS_APPLIED
    END_GROUP = L1G_PRODUCT_METADATA
END_GROUP = METADATA_FILE
END
```

# Appendix 4 - Environment Waikato sample analysis methods and data

| Code | Name | Units | Description |
|---|---|---|---|
| CHLA | Chlorophyll A | g/m³ | Acetone extraction. Spectroscopy. APHA 10200 H. |
| Cond | Conductivity - Lab Meter | mS/m @25"C | Measured in lab by meter @ 25"C. APHA Method 2510B |
| Depth | Depth - From Water Surface | m | Distance from water surface to measurement or sampling point |
| DRP | Dissolved Reactive Phosphorus | g/m³-P | Filtered sample. Molybdenum blue colorimetry. Discrete analyser. APHA 4500-P E (modified for manual analysis). |
| NH4 | Ammoniacal Nitrogen | g/m³-N | Filtered Sample. Colorimetry, Phenolhypochlorite. Discrete Analyser. APHA Method 4500-NH3 F (modified from manual analysis) (NH4-N = NH4-N + NH3-N). |
| NNN | Nitrate+Nitrite Nitrogen FIA | g/m³-N | Total Oxidised Nitrogen. Automated cadmium reduction, flow injection analyser. APHA 4500 NO3 I (proposed). NO2 plus NO3. |
| pH | pH - Lab Meter | pH | Measured in lab by meter. APHA Method 4500-H+ B. |
| SchiDisk | Secchi Disk | m | Visibility of standard disc |
| SSDirect | Suspended Solids - direct samp | g/m³ | Sampled directly, dried at 104c APHA Method 2540D |
| TKN | Total Kjeldahl Nitrogen | g/m³-N | Sulphuric Acid digestion with copper sulphate catalyst, phenol/hypochlorite colorimetry (discrete analyser). APHA 4500-Norg C (modified), 4500-NH3 F. |
| TotDepth | Depth - Total Water Depth | m | Total depth of water body |
| TP | Total Phosphorus | g/m³-P | Acid Persulphate digestion, ascorbic acid colorimetry. Discrete analyser. APHA 4500-P E (modified from manual analysis). |
| Turb-N | Turbidity - HACH 2100N | NTU | Nephelometry. Hach 2100N meter. APHA Method 2130B |
| VSS | Volatile Suspended Solids | g/m³ | GF/C filtration, ashed @ 550"C. APHA 2540 G. |

| Full Name | Date | Chl *a* | Cond | DRP | NH4 | NNN | pH | TSS | TKN | TP | Turb-N | VSS | Secchi |
|---|---|---|---|---|---|---|---|---|---|---|---|---|---|
| Lake Ngaroto | 28/03/2000 13:55 | 0.106 | 19.4 | 0.006 | 0.02 | 0.004 | 8.1 | 21 | 1.80 | 0.109 | 20.0 | 9 | |
| Lake Rotokauri | 28/03/2000 15:50 | 0.224 | 14.7 | < 0.004 | 0.02 | 0.004 | 9.4 | 30 | 3.08 | 0.152 | 54.3 | 23 | |
| Lake Rotomanuka | 28/03/2000 10:40 | 0.009 | 18.0 | 0.005 | < 0.01 | < 0.002 | 7.5 | 2 | 0.73 | 0.037 | 2.93 | 3 | |
| Rotomanuka Lake Gin | 28/03/2000 12:00 | 0.431 | 22.3 | 0.010 | < 0.01 | 0.006 | 7.3 | 33 | 2.93 | 0.210 | 24.6 | 29 | |
| Lake Waahi | 29/03/2000 10:50 | 0.008 | 41.6 | < 0.004 | 0.01 | < 0.002 | 8.1 | 13 | 0.68 | 0.039 | 9.70 | 5 | |
| Lake Waahi Weavers Basin | 29/03/2000 11:10 | 0.013 | 41.4 | < 0.004 | < 0.01 | < 0.002 | 8.2 | 11 | 0.67 | 0.023 | 7.73 | 6 | |
| Lake Waikare | 29/03/2000 13:10 | < 0.02 | 18.3 | 0.011 | 0.01 | 0.004 | 7.6 | 309 | 1.60 | 0.396 | 362 | 41 | |
| Lake Waikare Flood Control Gates | 29/03/2000 12:20 | | | | | | | 344 | | | 399 | | |
| Lake Serpentine North | 27/08/2002 15:35 | 0.021 | 15.8 | 0.005 | 0.01 | 0.018 | 7.1 | 2 | 0.98 | 0.026 | 1.77 | 2 | 1.60 |
| Lake Maratoto Center | 27/08/2002 11:05 | 0.008 | 15.2 | 0.005 | 0.12 | 0.274 | 5.1 | 2 | 1.18 | 0.031 | 1.64 | 2 | 0.95 |
| Lake Rotomanuka | 27/08/2002 13:50 | 0.023 | 17.0 | 0.004 | 0.10 | 0.211 | 7.4 | 6 | 0.86 | 0.026 | 2.91 | 3 | 1.63 |
| Lake Waahi Weavers Basin | 28/08/2002 11:15 | 0.034 | 24.8 | < 0.004 | 0.01 | 0.196 | 7.6 | 15 | 0.67 | 0.041 | 8.29 | 6 | 0.50 |
| Lake Waahi | 28/08/2002 10:30 | 0.026 | 26.3 | 0.004 | < 0.01 | 0.221 | 7.8 | 17 | 0.72 | 0.034 | 11.7 | 5 | 0.38 |
| Lake Waikare | 28/08/2002 15:50 | 0.133 | 14.4 | 0.004 | 0.03 | 0.007 | 7.5 | 219 | 2.29 | 0.475 | 198.0 | 48 | 0.10 |
| Lake Waikare Flood Control Gates | 28/08/2002 15:15 | | | | | | | 227 | | | 217.0 | | |